The Mars system revealed by the Martian Moons eXploration mission

Kazunori Ogohara, Hiromu Nakagawa, Shohei Aoki, Toru Kouyama,
Tomohiro Usui, Naoki Terada, Takeshi Imamura, Franck Montmessin, David
Brain, Alain Doressoundiram, et al.

HAL Id: insu-03510824
https://insu.hal.science/insu-03510824

FULL PAPER

The Mars system revealed by the Martian Moons eXploration mission

Kazunori Ogohara[1*] , Hiromu Nakagawa[2], Shohei Aoki[3,4], Toru Kouyama[5], Tomohiro Usui[6], Naoki Terada[2], Takeshi Imamura[7], Franck Montmessin[8], David Brain[9], Alain Doressoundiram[10], Thomas Gautier[8], Takuya Hara[11], Yuki Harada[12], Hitoshi Ikeda[13], Mizuho Koike[14], François Leblanc[15], Ramses Ramirez[16,17,25], Eric Sawyer[18], Kanako Seki[19], Aymeric Spiga[20,21], Ann Carine Vandaele[22], Shoichiro Yokota[23], Antonella Barucci[10] and Shingo Kameda[24]

Abstract

Japan Aerospace Exploration Agency (JAXA) plans a Phobos sample return mission (MMX: Martian Moons eXploration). In this study, we review the related works on the past climate of Mars, its evolution, and the present climate and weather to describe the scientific goals and strategies of the MMX mission regarding the evolution of the Martian surface environment. The MMX spacecraft will retrieve and return a sample of Phobos regolith back to Earth in 2029. Mars ejecta are expected to be accumulated on the surface of Phobos without being much shocked. Samples from Phobos probably contain all types of Martian rock from sedimentary to igneous covering all geological eras if ejecta from Mars could be accumulated on the Phobos surface. Therefore, the history of the surface environment of Mars can be restored by analyzing the returned samples. Remote sensing of the Martian atmosphere and monitoring ions escaping to space while the spacecraft is orbiting Mars in the equatorial orbit are also planned. The camera with multi-wavelength filters and the infrared spectrometer onboard the spacecraft can monitor rapid transport processes of water vapor, dust, ice clouds, and other species, which could not be traced by the previous satellites on the sun-synchronous polar orbit. Such time-resolved pictures of the atmospheric phenomena should be an important clue to understand both the processes of water exchange between the surface/underground reservoirs and the atmosphere and the drivers of efficient material transport to the upper atmosphere. The mass spectrometer with unprecedented mass resolution can observe ions escaping to space and monitor the atmospheric escape which has made the past Mars to evolve towards the cold and dry surface environment we know today. Together with the above two instruments, it can potentially reveal what kinds of atmospheric events can transport tracers (e.g., H_2O) upward and enhance the atmospheric escape.

Keywords: Mars, Mars system, Paleoclimate, Atmospheric escape, Water cycle, Dust cycle, Transport process

*Correspondence: ogohara@cc.kyoto-su.ac.jp
[1] Faculty of Science, Kyoto Sangyo University, Motoyama, Kamigamo, Kita-ku, Kyoto, Japan
Full list of author information is available at the end of the article

Ogohara *et al. Earth, Planets and Space*   (2022) 74:1

Page 2 of 32

Graphical Abstract
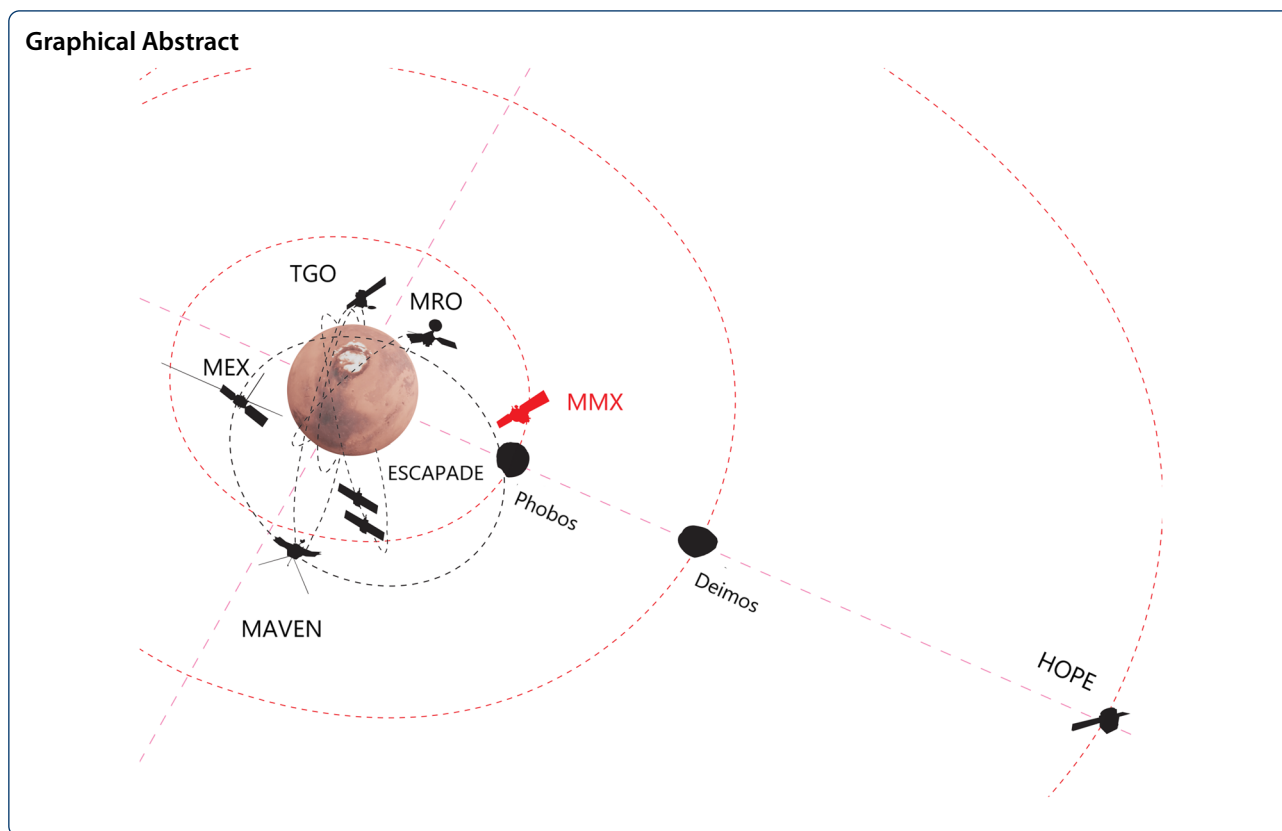
Introduction

Mars is the planet most similar to the Earth in the solar system in that it has a solid surface and an appreciable amount of atmosphere with moderate temperatures, and that there is evidence of liquid water activity, volcanic activity and a possible habitability. In recent decades many Mars missions have been conducted to reveal the planet's evolution and the current climate. Though the current Mars is a dry and cold world that includes a significant amount of frozen surface/subsurface water resources, geological evidence obtained by the spacecraft suggests that Mars may have sustained a wet and warm world in the past under the influence of a greenhouse effect (e.g., Ramirez and Craddock 2018). The transition to the current climate should have been driven by a combination of various physical/chemical processes, such as degassing, escape of volatiles to space, loss of the intrinsic magnetic field, exchange of water and other volatiles between the atmosphere and the crust, photochemistry, radiative transfer and atmospheric circulation. A possible example of strong coupling between different processes is the recent discovery of the apparent response of escaping ion fluxes to the upward transport of dust and water in the lower atmosphere (Heavens et al. 2018). The growing global interest in the history of the Martian surface environment motivated us to develop a Mars observation plan in the MMX (Martian Moons eXploration) mission aiming to disentangle the coupling among different processes, thereby assessing the roles of short-term elementary processes in the atmosphere and in the circum-Mars space in the long-term evolution of the Martian environment.

MMX is the third sample return mission of JAXA (Japan Aerospace Exploration Agency) (Kuramoto et al. 2021). The spacecraft will conduct close-up observations of the Martian satellites Phobos and Deimos, collect samples from Phobos, and bring them back to the Earth to reveal the origin of the two moons. In addition, MMX will conduct remote observations of the Martian atmosphere and surface and in situ measurements of volatiles escaping to space during the 3-year Mars orbiting phase. We take advantage of MMX's unique orbit around Mars: the equatorial high-altitude orbit will enable continuous remote monitoring of short-timescale phenomena in the atmosphere and increase opportunities of the measurement of low-energy ion outflows in the shadows of Mars and Phobos. The samples brought back to the Earth are expected to contain particles ejected from the Martian surface by asteroid impacts, from which information on early Mars will be retrieved. Combining this broad range

Ogohara *et al. Earth, Planets and Space*   (2022) 74:1

Page 3 of 32

of information will allow for an integrated understanding of Mars system that consists of Mars, its moons, and the circum-Mars space. For example, the transport of water across the atmosphere from the surface to space will be tracked with an infrared imaging spectrometer and an ion spectrometer, and this knowledge of water transport, combined with isotopic fractionation analysis of returned Mars samples, will allow us to develop a scenario of the environmental evolution of Mars. The spacecraft will be launched in 2024, put into a Martian orbit in 2025, stay in orbit around Mars until 2028, and return to the Earth in 2029. The detail of the mission sequence will be given by another paper in this issue.

Currently quite a few Mars missions are ongoing. They include Mars Odyssey, Mars Express (MEX), Mars Reconnaissance Orbiter (MRO), Curiosity rover, Mangalyaan orbiter, Chinese Tianwen 1 mission, Mars Atmosphere and Volatile Evolution (MAVEN), ExoMars Trace Gas Orbiter (EMTGO), and InSight lander. The Hope orbiter planned by United Arab Emirates will start remote observations of the Martian atmosphere from a high-altitude equatorial orbit in 2021. Mars sample return (MSR) mission is also currently under consideration to bring back samples from Mars (Beaty et al. 2019). The Mars observations in MMX are complementary to those missions in several aspects, such as the observation wavelength, the spatial resolution in global imaging, the sensitivity to low energies and the mass resolution in ion measurements, and the sample return to the Earth.

In this paper, we describe the science goals of the mission and the observation strategies. We describe the mission objectives related to the Mars science in the next section. The "Scientific background and key requirements for observation" section reviews the previous studies on the Martian paleoclimate, atmospheric escape and the transport processes in the atmosphere. What and how are understood from Martian samples accumulated on Phobos are summarized in the "Martian sample on the Phobos surface" section, the observation plan and the instruments in the "Mars observation by MMX" section, and the synergy with other Mars missions in the "Synergy with other missions" section. A summary is given in the last section.

Mission definition regarding the Mars environmental history

We are motivated to plan MMX by the growing global interest in the evolution of the Martian environment as mentioned in the "Introduction" section. This is reflected in one of the scientific goals (SGs) of MMX. The first of SGs (SG-1) is related to studies on the Martian moons and the understanding of the planetary system formation and material transport in the solar system (Kuramoto

et al. 2021). The second scientific goal of the MMX (SG-2) is:

- From the viewpoint of the Martian moons, clarify the driving mechanism of the transition of the Mars-moon systems and add new knowledge to the evolution history of Mars.

What is crucial for studies on the evolution of the planetary surface environment is to directly observe the history as geologists have reconstructed the history of the terrestrial environment from rock or sediment samples. Another important approach is to understand the phenomena seen in the atmosphere and circum-Mars space today and infer the past from them. Thus, SG-2 is broken down into three medium objectives (MOs). Table 1 provides an overview of the relationship between the SG, MOs and related science themes. The first MO is associated with the surface processes of the airless small body (i.e., Phobos) and the other two MOs cover the Mars environmental evolution:

- MO-2.2: add new findings and constraints on the history of changes in the Martian surface,
- MO-2.3: constrain the mechanisms of material circulation in the Martian atmosphere affecting the transitions in the Martian climate.

One of methods to achieve MO-2.2 is to restore the paleoclimate changes from Martian samples that have been accumulated on the Phobos surface (Hyodo et al. 2017). The other is estimation of the past atmospheric escape based on the present observations. They are expected to be achieved by analyses of Martian samples on Phobos returned to Earth and observations of the atmospheric escape. MO-2.3 covers understanding of the efficient upward transport processes required for efficient H_2O escape from the top of the atmosphere. MO-2.3 is expected to be achieved by continuous full-disk monitoring of Mars with visible and infrared wavelengths. Observations of distributions of dust, ice clouds, and water vapor with higher temporal and spatial resolutions than the previous observations are necessary for MO-2.3.

Previous studies on the three science themes, paleoclimate of Mars restored from samples on Phobos, the Martian atmospheric escape, and transport mechanisms in the present Martian atmosphere, associated with the MOs are reviewed in the next section. Plans of the analyses of the samples and expected findings are described in detail in the "Martian sample on the Phobos surface" section. Although the orbit of the spacecraft and scientific payload are briefly introduced for the reviews in the next section, they are fully described in the "Mars observation

Ogohara *et al. Earth, Planets and Space*　　(2022) 74:1

Page 4 of 32

Table 1 Relation between the science goal, medium objectives and related science themes

Science goal	Medium objective	Science theme	Measurement
SG-2: from the viewpoint of the Martian moons, clarify the driving mechanism of the transition of the Mars-moon systems and add new knowledge to the evolution history of Mars	**MO-2.2:** add new findings and constraints on the history of changes in the Martian surface	Paleoclimate restored from Martian samples on Phobos surface	Martian samples accumulated on the Phobos surface
		History of changes in the H_2O and CO_2 reservoirs of Mars	Ions escaping from the atmosphere including cold ions
	MO-2.3: constrain the mechanisms of material circulation in the Martian atmosphere affecting the transitions in the Martian climate	Material transport processes in the present Martian atmosphere	Continuous monitoring of the behavior of dust, clouds and water vapor with high temporal and spatial resolutions

See Kuramoto et al. (2021) for details of SG-1, MO-1, and MO-2.1

Ogohara *et al. Earth, Planets and Space*   (2022) 74:1

Page 5 of 32

by MMX" section. While they have been designed to make sure of the other MOs regarding SG-1, it is emphasized in the following sections that they are also suitable for observations of the Martian atmosphere and circum-Mars space regarding the above MOs and distinguished from other missions.

Scientific background and key requirements for observation

Martian paleoclimate

Mars is a cold and dry planet that exhibits below-freezing mean surface temperatures that are akin to those in many portions of Antarctica (e.g., Spanovich et al. 2006). However, this frigid present Mars contrasts heavily with the much warmer and wetter world that observations (both orbital and rover) suggest existed ~ 3.5–4 Gyr ago (e.g., Masursky 1973; Craddock and Howard 2002; Ramirez and Craddock 2018). The ancient highlands, which represent the oldest terrains on Mars that cover ~ 2/3 of the planet, abound with fluvial features, including deltas, alluvial fans, possible ancient shorelines, and most famously, the valley networks (e.g., Masursky 1973; Craddock and Howard 2002; Fassett and Head 2008a, b; Howard et al. 2005; Irwin et al. 2011; Usui et al. 2020).

Although climate models simulate the current climate quite well (e.g., Fenton et al. 2007; Pottier et al. 2017; Haberle et al. 2019a), this warmer and wetter early Mars has been a challenge to explain. As a result of its larger orbital distance and the faint young sun, early Mars 4 Gyr ago receives only ~ 32% the incident flux that our planet does. Thus, a dense atmosphere with a very strong greenhouse effect would have been required to sustain stable bodies of liquid water on the Martian surface.

Mars may have initially accreted ~ 10 bars of CO_2 based on a simple mass-radius scaling from Earth's primordial inventory (e.g., Ramirez and Craddock 2018). This is enough CO_2 to solve the climate paradox even though other processes, including atmospheric escape and volcanic outgassing, would have led to a net decrease in atmospheric pressure over time (e.g., Tian et al. 2010; Kurokawa et al. 2018). Indeed, atmospheric CO_2 pressures exceeding ~ 5 bar 3.8 Gyr ago would have yielded mean surface temperatures above the freezing point of water (e.g., Pollack et al. 1987). However, these early calculations had neglected CO_2 condensation, which was shown to reduce tropospheric lapse rates and decrease mean surface temperatures to ~ 220–230 K (e.g., Kasting 1991; Tian et al. 2010; Ramirez et al. 2014). Thus, a different mechanism would be needed to resolve the climate conundrum.

Subsequent calculations employing CO_2 clouds' scattering greenhouse effect showed that warm surface temperatures were achievable for CO_2 cloud coverage approaching 100% (Forget and Pierrehumbert 1997). However, this warming is drastically reduced at more realistic cloud fractions (~ 50%) (Forget et al. 2013). Plus, models that employ more accurate multi-stream radiative transfer schemes predict a much weaker CO_2 cloud greenhouse effect than that estimated with traditional two-stream approaches (Kitzmann 2016).

Similar complications were found for upper tropospheric cirrus clouds composed of water vapor. One study predicts that impact-induced cirrus clouds that consist of 10 micron or larger sized particles could generate transiently warm conditions (e.g., Urata and Toon 2013). Again, significant warming was possible only for cirrus cloud fractions exceeding ~ 75%, which is unrealistically cloudy for a potentially habitable planet with both rising and subsiding air (Ramirez and Kasting 2017). A recent study argues that significant warming is possible at lower cloud fractions if cirrus clouds can form in the stratosphere (Turbet et al. 2020a). However, this scenario is extremely unlikely because the stratosphere is dry and cirrus cloud formation is disfavored (Ramirez and Kasting 2017).

Thus, the difficulty of warming early Mars with just CO_2 and H_2O has led various investigators to consider whether the surface geology could have formed in a cold climate instead. This has spawned various cold and icy early Mars scenarios that invoke transient warming episodes caused by external events, including volcanic eruptions, meteoritic impacts, obliquity changes, methane bursts, or climate limit cycles (e.g., Segura et al. 2002, 2008; Ehlmann et al. 2011; Urata and Toon 2013; Forget et al. 2013; Kite et al. 2013, 2020; Wordsworth et al. 2013, 2015; Batalha et al. 2016; Haberle et al. 2019b; Steakley et al. 2019; Hayworth et al. 2020). It is worth noting that the notion of a permanently cold and icy early Mars has been questioned in recent years (e.g., Craddock and Howard 2002; Ramirez and Craddock 2018). For example, such mechanisms (to date) cannot produce the water amounts necessary to explain the widespread fluvial erosion, including the valley networks (e.g., Davis et al. 2016; Ramirez and Craddock 2018). Also, both rover and orbital evidence have shown no unambiguous evidence of extensive glaciation, whether wet- or dry-based, anywhere in valley network terrains (e.g., Burr et al. 2010; Grotzinger et al. 2015; Davis et al. 2016, 2019). Such observations have led to an increase in our understanding and contributed to the recent increase in solutions that favor various transiently and continuously warm scenarios over those that advocate a permanently cold and icy early Mars (e.g., Ramirez and Craddock 2018).

Nevertheless, it is now understood that the combined greenhouse effect of CO_2 and H_2O, even with clouds, does not provide enough warming to solve the

Ogohara *et al. Earth, Planets and Space*   (2022) 74:1

Page 6 of 32

early Martian climate problem. Some investigators have argued that secondary greenhouse gases could have provided that additional warming. Sulfur dioxide (SO_2), for instance, is an effective warming agent in a CO_2-dominated early Martian atmosphere (e.g., Postawko and Kuhn 1986; Mischna et al. 2013; Halevy and Head 2014; Kerber et al. 2015). However, not only does sulfur form long chains that reflect away incoming radiation, but SO_2 rains out of the atmosphere as temperatures warm, severely limiting its effectiveness (e.g., Tian et al. 2010).

Other gases have been considered as well. Using data suggesting potentially oxidizing conditions at Gale crater, Ito et al. (2020) posit that hydrogen peroxide (H_2O_2) could have been this potent secondary greenhouse gas. That said, an extremely high (and likely implausible) degree of supersaturation would have been required to warm the planet and offset photochemical destruction (Ito et al. 2020).

Another important greenhouse gas combination is CO_2–CH_4, which has a relatively strong greenhouse effect at high enough pressures (e.g., Ramirez et al. 2014; Wordsworth et al. 2017). However, absorption at solar wavelengths forms upper atmospheric temperature inversions that negate some of this warming (Ramirez et al. 2014; Wordsworth et al. 2017). Although initial estimates of CO_2–CH_4 collision-induced absorption (CIA) had suggested that ~ 10% CH_4 in a 2-bar CO_2 atmosphere could have nearly produced the required climates (Wordsworth et al. 2017), subsequent experimental estimates found that CO_2–CH_4 CIA is much weaker than previously estimated, further weakening the plausibility of this solution (Turbet et al. 2019, 2020b).

Ramirez et al. (2014) had originally proposed that a CO_2–H_2 greenhouse could have warmed early Mars. This was based on analyses of Martian meteorites suggesting a highly reducing early mantle (e.g., Shearer et al. 2006; Nakada et al. 2020; Wadhwa et al. 2001), permitting percent levels of volcanically outgassed hydrogen to accumulate in the atmosphere in spite of high atmospheric escape rates (Ramirez et al. 2014). Revised calculations suggest that atmospheres consisting of ~ 3–10% H_2 and 1–2 bars of CO_2 may have been sufficient to warm early Mars (Wordsworth et al. 2017; Ramirez 2017). Other calculations indicate that such CO_2–H_2 atmospheres are photochemically stable (Batalha et al. 2015). However, as with methane, CO_2–H_2 CIA had been significantly overestimated (Turbet et al. 2019, 2020b). That said, even with the revised absorption cross sections, this greenhouse solution remains very promising. For instance, warm climates can be achieved with just 5% H_2 in a 2-bar CO_2 atmosphere (Turbet et al. 2020b; Godin et al. 2020).

However, these previous CO_2–H_2 computations were performed using simple radiative–convective climate models. Recent studies utilizing advanced climate models have incorporated oceans and calculated estimated precipitation (rain, snow) rates (Ramirez et al. 2020; Kamada et al. 2020). The warm simulations in both studies yield hydrogen and carbon dioxide partial pressures that are consistent with those predicted by radiative–convective models. They also find that a warm early Mars with a large northern ocean would have likely had an arid to semi-arid climate (Ramirez et al. 2020; Kamada et al. 2020). Valley network formation would have been brief, nearly global, and finished within 10^4–10^7 years (Ramirez et al. 2020; Kamada et al. 2020), which is consistent with geologic inferences (e.g., Hoke et al. 2011; Orofino et al. 2018). In addition, Ramirez et al. (2020) find that precipitation rates are negligible for warm climates with small oceans. Thus, they conclude that a large ocean may have been necessary to produce a hydrologic cycle that was robust enough to form the observed surface geology. It is possible that Mars samples retrieved from Phobos could elucidate the earliest period of Mars (the "Martian sample on the Phobos surface" section), including the amount of water that may have existed during these ancient times.

Atmospheric escape

The cumulative effect of the atmospheric erosion due to the external forcing, such as solar radiation and solar wind, is regarded as one of the plausible candidates of the drastic climate change from warm and wet to cold and dry environment. Especially, the lack of a global magnetic field on Mars must have a significant impact on the atmospheric escape. The weak magnetosphere would have allowed solar wind to strip away much of its atmosphere to space. There have been proposed a variety of processes of the atmospheric escape from Mars (e.g., Shizgal and Arkos 1996; Chassefiere and Leblanc 2004).

The lack of a global magnetic field means that the upper atmosphere of Mars is directly exposed to the solar wind, leading to erosion of ionized gasses from the top of the atmosphere through various processes driven by the solar wind interaction. The Soviet Mars 2, 3, and 5 spacecraft first measured the ion escape from Mars and also identified characteristic plasma boundaries such as bow shock (e.g., Vaisberg and Smirnov 1986, and references therein). Later Phobos 2 spacecraft also measured a significant loss of ionospheric ions through the magnetotail (e.g., Lundin et al. 1989; Lundin et al. 1990; Lundin and Dubinin 1992). These spacecrafts estimated ion escape rates to be of the order of 1024–1025 s^{-1}, which correspond to evacuation of the total oxygen content in the present-day atmosphere of Mars in less than

Ogohara *et al. Earth, Planets and Space* (2022) 74:1

Page 7 of 32

108–109 years. Recently the Ion Mass Analyser (IMA) instrument, one of the Analyser of Space Plasma and Energetic Atoms (ASPERA-3) package aboard ESA's Mars Express (Barabash et al. 2006), has successfully measured heavy ions such as O^+, O_2^+, and CO_2^+ escaping through the induced magnetotail (e.g., Carlsson et al. 2006; Lundin et al. 2009). IMA has measured ion distribution functions since 2004 to date, and the > 16 years of observations have provided many opportunities to study the ion escape for characteristic solar events and seasonal changes (e.g., Futaana et al. 2008; Dubinin et al. 2009; Edberg et al. 2010; Hara et al. 2011; Yamauchi et al. 2015). The long-term dataset of IMA has also provided comprehensive views in the heavy ion escape rates from Mars, varying within 1024 s^{-1} order of magnitude under a variety of external conditions in terms of the solar wind and solar EUV flux (e.g., Lundin et al. 2008; Nilsson et al. 2010, 2011; Ramstad et al. 2015, 2017, 2018).

Recent observations of the Suprathermal and Thermal Ion Composition (STATIC) instrument (McFadden et al. 2015) aboard NASA's MAVEN spacecraft resolved two distinctive ion escape channels, the plume channel along the convective electric field of the solar wind and the tail channel along the magnetotail (Dong et al. 2015; Brain et al. 2015), which agrees with theoretical studies (e.g., Fang et al. 2008). Dong et al. (2015, 2017) also estimated the O^+ ion escape rates of the orders of 1023 s^{-1} and 1024 s^{-1} through the plume and tail channels, respectively. The simultaneous ion and magnetic field measurements of MAVEN also provided characteristic features linked to the ion acceleration and escape such as classical pickup ions in the solar wind (Rahmati et al. 2017, 2018; Masunaga et al. 2017), their reflections in the magnetosheath and resulting ion beams above the bow shock (Masunaga et al. 2016, 2017), magnetic reconnections in the tail and dayside ionosphere (Harada et al. 2015, 2017, 2018, 2020), vortex structures likely caused by the Kelvin–Helmholtz instability (Ruhunusiri et al. 2016), and flux ropes containing heavy ions near the crustal magnetic field (Hara et al. 2015, 2016).

Modeling efforts have been also made to understand the observational results for decades (e.g., Brain et al. 2010, and references therein). The modeling works today can reproduce characteristic plasma environments around Mars in a good agreement with observations (e.g., Ma et al. 2004, 2017; Fang et al. 2008, 2017) and calculate global ion escape rates for the major ion species at present-day Mars (e.g., Ma et al. 2004, 2015; Modolo et al. 2016; Dong et al. 2018). Such modeling works have been also applied to ancient Mars (e.g., Terada et al. 2009; Sakai et al. 2018, 2020).

As reviewed above, comprehensive observations of the Martian upper atmosphere by previous Mars missions and modelling works have provided the oxygen ion escape rate from present-day Mars and estimate of its integrated loss through time, and similar efforts have been also made for other escape processes such as Jeans' escape of hydrogen, photochemical and sputtering losses of oxygen (e.g., Jakosky et al. 2018, and references therein). However, it is not yet understood whether these oxygen escapes originate from H_2O or CO_2 of the Martian atmosphere. Although theoretical estimate of carbon escape rate from present-day Mars is 1–2 orders of magnitude smaller than those of H and O (Gröller et al. 2014; Cui et al. 2019), it could have been comparable to or even greater than the O escape rate in the past (Amerstorfer et al. 2017). In order to understand the integrated losses of H_2O and CO_2 through time, determining not only oxygen and hydrogen escape rates, but also carbon escape rate at Mars today and their extrapolation backward in time are equally important. To date a few studies established mass separation methods for IMA and STATIC measurements and identified escaping O^+, O_2^+ and CO_2^+ ions (Carlsson et al. 2006; Inui et al. 2018, 2019) and many multispecies simulation results provided global escape rates of these ion species (e.g., Ma et al. 2004). However, these species could be resolved further into minor species at their neighboring masses such as C^+, N^+, Ar^+, and so on. In addition, recent MAVEN observations in the Mars shadow have revealed cold ion outflow rates that would significantly contribute to the total outflow rate (Inui et al. 2018, 2019). However, the understanding of the cold ion outflow is still shrouded in mystery owing to lack of measurements and difficulty in validation by theoretical studies (e.g., Dubinin et al. 2011; Lundin 2011; Harnett and Winglee 2006; Ma et al. 2004). Precise estimates of the atmospheric and water amounts that have escaped to space in the past remain elusive.

Extracting carbon from the dominant ion populations, such as oxygen ions at present day requires accurate mass separation of these species and has been a challenging subject. The mass spectrum analyzer (MSA) aboard MMX has advantages over its preceding measurements of ion outflows from Mars in terms of (1) high mass resolution measurements of escaping ions at high altitudes and (2) cold ion measurements in the shadows of Mars and Phobos. MSA will achieve unprecedented high mass resolution observations with M/dM > 100 at high altitudes (Phobos orbit) to measure ion outflows including tenuous ions such as C^+, N^+, and Ar^+. MSA will also attempt to measure isotope ratios of O^+ and C^+ and deduce their fractionation factors to understand the long-term evolution of the Martian atmosphere.

The new comprehensive measurements of carbon-, oxygen-, and hydrogen-bearing ion species with high mass resolution of MSA will provide crucial constraints

Ogohara *et al. Earth, Planets and Space* (2022) 74:1

Page 8 of 32

on H_2O and CO_2 escape rates and its extrapolation backward in time. The extrapolation can be done using a simple approach in Jakosky et al. (2018), i.e., adopt already published models for the time history of escapes, and apply a scaling factor so that the models match the escape rates measured today by the spacecraft. Or, it may be directly derived from measurements of the dependence of the escape rates on solar conditions (e.g., Ramstad et al. 2018). Furthermore, as will be discussed in "Martian sample on the Phobos surface" section, the long-term evolution of oxygen and carbon isotopic ratios in the Martian surface environment may be constrained by the samples brought back by MMX. Combined with the isotopic fractionation factors of outflow ions deduced by MSA, the evolutionary history of the amount of H_2O and CO_2 reservoirs in the Martian surface environment is expected to be further constrained (e.g., Jakosky and Jones 1997).

As for cold ion measurements, MMX will frequently enter the shadows of Mars and Phobos, which will provide a unique opportunity to measure cold ions escaping from Mars. In the shadows, spacecraft is negatively charged, allowing it to measure low-energy ions that cannot be detected in sunlit regions. Observations in the shadow of Phobos will enable the first measurements of cold ions outside the Martian shadow. Previous observations showed that the acceleration mechanisms of the cold planetary ions depend both on tailward distance from Mars and solar wind conditions (e.g., Nilsson et al. 2012; Inui et al. 2019). MSA observations at the fixed tailward distance will provide unique data to assess the effects of solar conditions on the cold ion escape process through the induced magnetotail. Simultaneous observations with other Mars orbiters such as MAVEN and ESCAPADE (ESCape and Plasma Acceleration and Dynamics Explorers) will add extra value to the MSA observations in this context. The knowledge of the solar variation dependence of the cold ion escape process is essential to derive an accurate extrapolation into the past. High mass resolution measurements by MSA also provide valuable opportunity to compare characteristics of different ion species such as O^+, C^+, N^+, and Ar^+, which will give us critical information to identify major acceleration mechanisms to cause cold planetary ion outflows from Mars.

Moreover, as shown by MAVEN, it is also possible to derive the neutral exosphere density from in situ pickup ion measurements (Rahmati et al. 2018) at distance where no direct measurement of the neutral exosphere is possible and where the neutral exosphere is essentially escaping. In another way, MSA will also have an indirect capability to reconstruct Mars' exospheric neutral escape thanks to its large energy range and mass resolution and

to track the dependency of this escape channel with respect to the solar conditions.

The atmospheric Martian He can be produced by radioactive decay of U and Th in the interiors of the planet followed by surface outgassing (Krasnopolsky and Gladstone 1996), by solar wind implantation (Stenberg et al. 2011) and lost by photo-ionization and acceleration by the solar wind convective electric field (Barabash and Norberg 1994) or by non-thermal escape (Gu et al. 2020). To reconstruct accurately the global balance of the atmospheric He sources can therefore provide key information on the origins of the atmospheric He and a constraint of the intensity of the surface outgassing. MSA by measuring the He^+ will quantify two key channels of the atmospheric He balance: Solar wind implantation (including the open question of solar wind reflexion at the bow shock (Chanteur et al. 2009)) and solar wind sweeping.

The multi-instrumental sciences of MMX will provide an ideal opportunity to reveal the fate of water of Mars. As will be described in "Fine structure and rapid transport processes of water and dust" section, MMX will measure dust activity and upward transport of water in the Martian atmosphere. At almost the same time, MMX will observe the outflow of ions into space. So, we can clarify the connection between the outflow of ions and the atmospheric events in the lower atmosphere such as dust storms and water ice clouds. Recent observations by Mars orbiters and space telescopes have revealed the importance of high-altitude water for hydrogen escape to space (e.g., Clarke et al. 2014; Chaffin et al. 2017; Heavens et al. 2018; Aoki et al. 2019; Stone et al. 2020; Masunaga et al. 2020). It has also been suggested that the oxygen loss rate may decrease during a dust storm (Lee et al. 2020). Coordinated observations of MSA and the other instruments (see "Instruments" section) aboard MMX will clarify a possible connection between the Martian atmosphere and atmospheric escapes.

Some portion of the escaping ions from the Martian atmosphere will impinge on the surface of Phobos and cause space weathering of the surface layer. We plan to identify the contributions to space weathering of escaping ions through tail and of plume ions, including C^+, N^+, etc., to understand the co-evolution of Mars and its moons (Yokota et al. 2021).

Fine structure and rapid transport processes of water and dust

The previous observations of the lower atmosphere have been mostly done by polar-orbiting spacecrafts (such as Mars Global Surveyor (MGS), MEX, MRO) (e.g., Smith 2002; Kleinböhl et al. 2009). These observations have provided global pictures of the atmospheric species and

Ogohara *et al. Earth, Planets and Space*   (2022) 74:1

Page 9 of 32

aerosols distributions at the Martian atmosphere; however, their diurnal variations have only been investigated using observations at (mostly) fixed local times in the interval 2–3 AM and PM. MEX is not sun-synchronous. So, it can cover all local times in principle, but it takes long time to do it. Thus, hourly development and decay of mesoscale to synoptic scale atmospheric events (such as horizontal water transport including surface–atmosphere interaction, clouds formation, and dust storms, etc.) have remained unclear. The more recent TGO mission already improved this coverage with its inclined orbit (74°) allowing different local times to be probed. The equatorial orbit of MMX, which is driven by the Phobos sample return goals, will be unique in this context. One of the main advantages of the MMX orbit is that we can monitor same regions for a few hours almost every day during a particular period (described in "Baseline operation" section), which allows us to reveal the rapid transport processes of the atmospheric species and aerosols with relatively high spatial resolution (typically 2–5 km/pixel); whereas, it is neither possible for the MMX orbit to observe the polar regions nor to cover all local times in the regions of interest in a single sol. Towards the MMX era, here we briefly review what the previous measurements revealed in terms of water vapor and dust fine structures and their rapid transport processes.

Previous observations have shown that a high variability governs the global-scale water vapor distribution. The seasonal variation of water vapor appears mainly controlled by atmospheric dynamics and sublimation–condensation process between the atmosphere and the polar regions (e.g., Smith 2002; Fouchet et al. 2007; Montmessin et al. 2017). Also, Mars' water cycle evolves in a steady-state with some interannual variability mostly visible during southern summer (Smith 2004). However, the water cycle remains overall more stable than dust since water sources or sinks are not directly stimulated by the occurrence of dust storms.

Progress in our understanding of the water cycle has been rapid over the last two decades, thanks to the continuous survey performed by several orbiters and also by the maturation of 3D Mars climate models (Navarro et al. 2014; Haberle et al. 2019a; Neary et al. 2020). However, some old questions have resisted interpretation so far. One of them concerns the exchange of water between the regolith and the atmosphere. The puzzling local maxima observed in the low-to–middle latitudes reported by Fouchet et al. (2007) can potentially be explained by dynamics, yet water locally trapped by the subsurface cannot be ruled out. In short, despite a large corpus of dedicated studies, the regolith's role in the water cycle remains largely elusive. Even if modelers have produced consistent simulations of Mars' water cycle without a regolith,

suggesting the latter could be neglected at first, observations have left a large gap in bringing the constraints needed to elucidate this role.

One key that could help filling this gap resides in monitoring the local time variation while producing global views of the water vapor column-abundance. That way a closure between the horizontal and the vertical fluxes of water could be tentatively undertaken and some source or sink at/in the surface could then be spotted.

However, the retrieval of water vapor during the nighttime is difficult, if not impossible, for most remote-sensing observations conducted so far (no Sun implies no signal in the near-infrared while the weak thermal contrast between the surface and the atmosphere at night and the colder temperature leave thermal infrared sensors "blind"). Some previous measurements implied that the water vapor abundances could vary daily by a factor of 2–3 (Titov 2002 and reference therein). In contrast, other studies show no significant local time variation (Maltagliati et al. 2011; Trokhimovskiy et al. 2015).

These previous observations were conducted in the context of polar orbits and had to compare data taken at different Mars years or locations to study local time variation. Thus, it has been difficult to directly explore the diurnal cycle except in the polar regions where it is possible to cover different local time in a single orbit (Melchiorri et al. 2009). The MMX Mars observations will investigate the local-time variation of column density of water vapor at low-to-middle latitudes by continuous monitoring from its equatorial orbit. Recent in situ measurements have suggested a strong diurnal variation of local water vapor abundances on the surface at low-to-middle latitudes (e.g., Savijärvi et al. 2019), and the MMX measurements will provide a comprehensive view on the surface–atmosphere interaction of water by remote-sensing observations.

Another piece of the water cycle puzzle still missing concerns its local distribution. Only two instruments—OMEGA onboard MEX and Compact Reconnaissance Imaging Spectrometer for Mars (CRISM) onboard MRO—have had capability to investigate mid-resolution maps of water vapor (< 5 km), but were limited in their total swath to a few hundred km, making it impossible to contextualize the observed fine structures (see e.g., Melchiorri et al. 2009). The latter authors identified a fine structure of water vapor enhancement correlated with surface albedo map, arguably caused by surface–atmosphere interactions. Maltagliati et al. (2008) investigated high-resolution maps of water vapor over the Tharsis volcanoes. They found a peculiar water vapor enrichment on the top of volcanoes that could be caused by local circulation around the volcanoes (e.g., Rafkin et al. 2002). Such a local upward topographically

Ogohara *et al. Earth, Planets and Space*   (2022) 74:1

Page 10 of 32

forced transport may contribute to the formation of water detached layers, as suggested in Heavens et al. (2019). The MMX observations of Mars will monitor water vapor at high spatial resolution and provide a global view that shall help better characterizing the existence of fine structures and of potential exchanges between the atmosphere and the regolith. The detailed capability of MMX Mars observations is described in the next section and summarized in Table 2.

Recent observational and modeling work about dust transport processes on Mars highlighted both the fine-scale structure of dust storms and the rapid vertical transport they imply. The key role played by the radiative warming by dust particles in dust storms has been recognized at all scales, from local to global (Heavens et al. 2019). This makes the dynamics of dust storm and dust transport processes very likely to be developing over a couple of hours, as shown both by modeling (e.g., "rocket dust storms", Spiga et al. 2013) and observations (e.g., "textured dust storms", Guzewich et al. 2017). One of the most striking recent results is the enhanced transport of water vapor to the upper atmosphere of Mars, and surge in atmospheric escape of hydrogen, especially during global dust storms (Fedorova et al. 2018, 2020; Vandaele et al. 2019; Aoki et al. 2019; Stone et al. 2020) in which dusty deep convection occurs (Heavens et al. 2018; Shaposhnikov et al. 2019; Neary et al. 2020). The MY34 (Mars Year 34) dust storm illustrated how strong and rapid vertical transport of dust particles can be (Bertrand et al. 2020) and how the diurnal variability of dust optical depth is stronger than initially thought, as a result of vertical and horizontal transport processes (Kleinböhl et al. 2020; Montabone et al. 2020; Liuzzi et al. 2020). Many of the aforementioned results and interpretations were, however, obtained from a combination of sun-synchronous orbital observations and atmospheric modeling. The complete life cycle of a dust storm, the rapid development of convective units within the storm cluster, and the vertical extent and magnitude of dust transport have never been observed on Mars. This is where the peculiar orbit and multi-instrumental payload of MMX may play a role in permitting to broaden the knowledge of dust transport processes on Mars.

Martian sample on the Phobos surface

MMX plans to collect a sample of at least 10 g from the regolith of Phobos (Usui et al. 2020). The surface of Phobos is likely to exhibit evidence of meteoritic ejecta from Mars (Ramsley and Head 2013; Nayak et al. 2016; Hyodo et al. 2019). The Martian ejecta on Phobos represent Martian topsoil accumulated over geologic time, which may include various materials different from Martian meteorites. Recent work by Hyodo et al. (2019) estimate that several hundreds of ppm of Martian ejecta is mixed within the Phobos regolith. Within a decade, MMX may collect rare Martian materials along with the Phobos regolith, providing new insights into the environment and possible habitability of early Mars. In this subsection, we briefly review what we currently know about the Martian surface evolution from the geological and mineralogical records on Mars and the geochemical records in Martian meteorites. Usui et al. (2020) summarizes the scientific importance of the Phobos sample. More specific strategies for the initial analysis and the curation process are proposed by Fujiya et al. (in prep.) in this same volume.

Geological and mineralogical records on the Martian surface indicate that the red planet was not red early in its history. Recent Mars exploration missions have reported conclusive evidence for the past existence of liquid water and a thicker atmosphere and the global-scale transition to the currently cold desert-like surface condition (e.g., Bibring et al. 2006; Carr and Head 2010; Ehlmann and Edwards 2014; Usui 2019a). The Noachian Martian ($> \sim 3.7$ Ga) terrains are characterized by significant fluvial erosions, dense valley networks, lakes and rivers, as well as active volcanism and massive impact cratering (e.g., Craddock and Howard 2002; Fasset and Head 2008). Secondary phyllosilicates, such as Fe/Mg smectite and chlorites were identified throughout Noachian regions (Bibring et al. 2006; Ehlmann et al. 2011; Ehlmann and Edwards 2014). The widespread occurrence of the fluvial landforms and the hydrous minerals suggest, episodically, if not continuously, warmer and water-rich conditions

Table 2 Summary of the MMX capability for Mars observations

Instrument	Spatial resolution[a]	Temporal resolution	Mass resolution	Targets
MIRS	~2.5 km	1 h		Dust, H_2O, CO, Water ice clouds, CO_2 ice clouds, surface pressure, O_2 dayglow
TENGOO	~35 m	1 min		Dust events, water ice clouds
OROCHI	~2.5 km	15 min		Dust events, water ice clouds
MSA		>4 s	M/ΔM~100	ion outflows including C^+, N^+, O^+, and Ar^+

[a] Spatial resolution at the sub-spacecraft point when observing from QSO

Ogohara *et al. Earth, Planets and Space* (2022) 74:1

Page 11 of 32

during the late Noachian/early Hesperian (e.g., Ramirez and Craddock 2018), although the nature of the ancient climate remains a matter of debate (see "Martian paleoclimate" section). During the late Noachian to early Hesperian, the surface mineralogy also gradually shifted from phyllosilicates to carbonate and sulfate-rich assemblages, suggesting monotonic acidification of the fluid chemistry (Ehlmann et al. 2011; Ehlmann and Edwards 2014; Usui 2019a). The overall geomorphologic and mineralogical findings indicate a global transition from an early Earth-like Mars to the currently cold desert-like surface. In contrast to the earlier periods, most Amazonian terrains (< ~ 3.0 Ga) are characterized by anhydrous oxide-rich mineralogy suggestive of scant fluvial activity, although massive amounts of water ice and/or icy sediment might be hidden beneath the surface (Usui 2019a).

Geochemical information obtained from Martian meteorites is another important clue. Most known Martian meteorites are basaltic or ultramafic in composition and subdivided into three mineralogical groups: shergottites, nakhlites and chassignites (McSween and McLennan 2014; McSween 2015 and references therein). Their Martian origin was originally determined via measuring the isotopic compositions of the trapped gases within impact-melted glasses from some meteorites (Bogard and Johnson 1983). The others are linked by oxygen three isotopic compositions (Clayton and Mayeda 1996) as well as other geochemical characteristics (e.g., Agee et al. 2013). Magmatic crystallization ages are relatively recent (~ 1.3 Ga to 0.2 Ga; Nyquist et al. 2001) and represent mostly anhydrous Amazonian conditions, although some rocks contain the trace aqueous weathering products that formed at the near-surface system (Bridges et al. 2019). On the other hand, a few old rocks have been classified as irregular Martian members, such as a 4.1 Ga orthopyroxenite, ALH 84001 (Mittlefehldt 1994; Lapen et al. 2010) and an ancient basaltic breccia, NWA 7034 and its paired meteorites (Agee et al. 2013). The various igneous lithologies found in the NWA 7034 series are likely to have formed by intensive magmatic and/or impact events during at Noachian age of 4.43 Ga to ~ 4.3 Ga (Humayun et al. 2013; Bellucci et al. 2015; Nyquist et al. 2016; Cassata et al. 2018), although their whole rocks experienced the prolonged thermal metamorphism during early to middle Amazonian period. Hence, only ALH 84001 is known to have preserved Noachian near-surface materials in its alteration deposits to date (e.g., Borg et al. 1999; Halevy et al. 2011; Bridges et al. 2019). Nevertheless, sporadic, but large variations of the formation and/or metamorphic ages of the Martian meteorites enable us to estimate the fate of the ancient Martian water cycle over time.

The atmospheric D/H ratio is one of the most informative tracers for the Martian surface evolution (Usui 2019b), as its isotopic fractionation likely reflects temporal variations in the near-surface hydrologic cycle and atmospheric escape. The current Martian atmosphere and the surface regolith are known to have a D/H ratio that is ~ 6–8 times higher than that of terrestrial ocean water (e.g., Owen et al. 1988; Webster et al. 2013; Leshin et al. 2013). Such extremely high D/H ratio resulted from a preferential escape of the lighter isotope (^1H), suggesting that the Martian atmosphere was irreversibly lost over geologic history (Lammer et al. 2013; Kurokawa et al. 2014). Igneous and/or secondary hydrous phases in the Martian meteorites record the past D/H ratio of the various water reservoirs. The igneous water (OH)-bearing minerals and hydrous glasses in the young (< 1 Ga) meteorites have comparable D/H ratio to the current Martian atmosphere (Greenwood et al. 2008; Hu et al. 2014), suggesting that their water reservoir was in equilibrium with the near-surface atmosphere. The D/H ratio of the Noachian crustal water recorded in the ALH 84001 was reported to ~ 4 times as high as the terrestrial value (Greenwood et al. 2008). This implies that the Martian atmosphere and surface water had been extensively lost prior to 4 Ga (Kurokawa et al. 2014), although modest D/H ratios were also proposed for ALH 84001 (Sugiura and Hoshino 2000; Boctor et al. 2003).

Along with the surface water records, the D/H ratio of the Martian primordial water is another essential piece of information for understanding the global evolution. Previous studies estimate that the Martian mantle has retained its primordial water, whose D/H ratio is similar to or slightly higher than the terrestrial water (Leshin 2000; Usui et al. 2012). However, the mantle water abundance may be quite low (< 100 ppm; Usui et al. 2012; McCubbin et al. 2016), at least in Martian meteorite source regions. In addition to the surface and interior (primordial) water, the existence of another water reservoir on current Mars is predicted (Usui et al. 2015; Mahaffy et al. 2015) based on D/H studies of Martian meteorites and hydrous minerals from 3 Ga Gale Crater mudstones. Subterranean water ice, icy sediments, and/or hydrated minerals are plausible candidates for this potential hidden Martian water, which has been kept isotopically isolated from the near-surface environment over geologic history. Indeed, massive ground ice layers have been geologically identified by recent observations (Mouginot et al. 2012; Dundas et al. 2018). If the hydrous subsurface has been retained under the dry, cold and oxidizing surface of Mars, ancient Martian life, if any, might have survived within the subsurface until today (Usui 2019a, b and references therein).

In addition to the D/H ratios, other atmophile components are important tracer of the Martian surface evolution. Compared to the terrestrial atmosphere, the present-day Martian atmosphere is characterized with isotopically heavy carbon dioxide (CO_2) with $\delta^{13}C = 46 \pm 4$ ‰ (Webster et al. 2013), dinitrogen (N_2) with $\delta^{15}N = 572 \pm 82$ ‰ (Wong et al. 2013) and noble gases such as $^{20}Ne/^{22}Ne = 10.1 \pm 0.7$ (Pepin 1991) and $^{36}Ar/^{38}Ar = 4.2 \pm 0.1$ (Atreya et al. 2013). Those are results of the complicated atmospheric evolutions via thermal and non-thermal escapes (e.g., ion pic up, sputtering, impact erosion) and replenishment by impacts and/or magmatism (Lammer et al. 2020). Lifetimes of N_2 and light noble gases are estimated as shorter than the age of Mars, indicating that their present-day isotopic compositions reflect the recent (< 4 Ga) atmospheric loss and input balance (Lammer et al. 2020). On the other hand, Xe in the Martian atmosphere is an important clue for the ancient environmental shift. Xenon, the heaviest noble gas with nine stable isotopes (124, 126, 128, 129, 130, 131, 132, 134, 136), is more difficult to escape compared to the lighter noble gases via mass-dependent thermal processes. Nevertheless, its isotopic compositions ($^nXe/^{132}Xe$) show significant fractionations both in the terrestrial and Martian atmosphere (Conrad et al. 2016; reviewed by Avice and Marty 2020). Such Xe fractionation can be attributed to the ancient hydrodynamic escape triggered by the EUV radiation from young Sun. Moreover, the Xe fractionation can also be caused by the ionic coupling with escaping hydrogen (H) originated from the surface water. Cassata (2017) reported that the 4 Ga atmospheric Xe trapped in ALH 84001 (and probably, NWA 7034, as well) seems to be already isotopically fractionated to the present level, suggesting that the Martian Xe had intensively escaped during early Noachian era, which had ceased prior to 4 Ga. This is opposite to the Earth case, where the atmospheric Xe continued to fractionate for ≥ 2 billion years, coupled with the surface water escape (Avice and Marty 2020). The early cessation of the Martian Xe fractionation indicates disappearance of the permanent liquid water on Mars prior to 4 Ga, which is consistent with the other geochemical and geological implications.

The case of Martian atmospheric nitrogen (N_2) appears to be somewhat different from the Xe evolution. Its present $^{15}N/^{14}N$ ratio is known ~ 1.6 times as heavy as the terrestrial value (i.e., $\delta^{15}N = 572 \pm 82$‰; Wong et al. 2013), although the Noachian atmosphere trapped in ALH 84,001 showed very little ^{15}N enrichments (Mathew and Marti 2001). It is suggested that the Martian $^{15}N/^{14}N$ ratio was elevated by later atmospheric evolution (< 4 Ga to present). Because of the lack of Martian surface samples aged betwee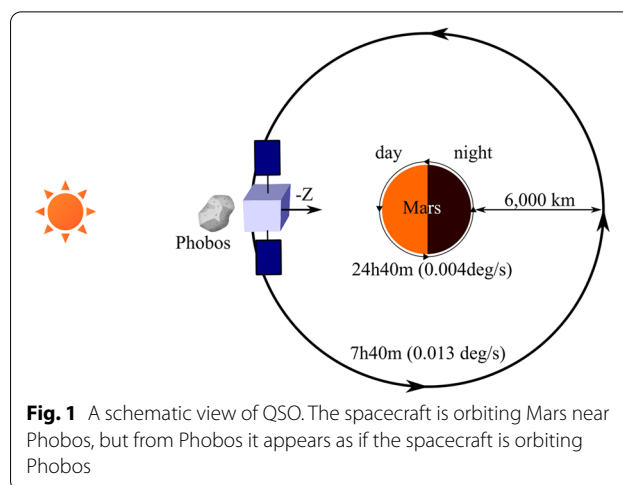n 4 and ~ 0.5 Ga, this evolution history remains unsolved. Meanwhile, some Martian meteorites and the Martian soils analyzed by MSL recently suggested the presence of "fixed nitrogen" such as nitrate and N-bearing organic matter (e.g., Kounaves et al. 2014; Stern et al. 2015; Koike et al. 2020), whose isotopic compositions would provide further constraint on the Martian surface evolution.

Isotopic composition of carbon ($^{13}C/^{12}C$) is somewhat more complicated. Carbon dioxide (CO_2) dominates the current Martian atmosphere and is involved in various planetary processes, including volcanic degassing, atmospheric escape, formation of carbonate minerals and organic matter and their possible preservation at the Martian subsurface system (Hu et al. 2015; Bridges et al. 2019; Kounaves and Oberlin 2019). Present-day Martian atmospheric CO_2 has heavy $^{13}C/^{12}C$ ratio of $\delta^{13}C = 46 \pm 4$ ‰ referenced to the Vienna Pee Dee belemnite (VPDB) analyzed by Curiosity rover (Webster et al. 2013). The heavy $^{13}C/^{12}C$ was also reported for young Amazonian-aged meteorite ($\delta^{13}C$ up to ~ 40‰; Carr et al. 1985), while Martian mantle-derived $^{13}C/^{12}C$ is estimated to be much lighter. The 4 Ga carbonates in ALH 84001 also has high $\delta^{13}C$ value of ~ 27 to 64 ‰ (Niles et al. 2005), probably reflecting the isotopically heavy Noachian atmosphere. If the ALH 84001 carbonates represent the 4 Ga atmospheric $\delta^{13}C$ value, the Martian atmosphere is inferred to have extensively escaped by that time and have been kept without severe change over the next ~ 4 billion years. On the other hand, Hu et al. (2015) consider that the Martian atmospheric $^{13}C/^{12}C$ records more recent (from 3.8 Ga to present) evolution, from which they estimate the atmospheric pressure of ≤ 1 bar for the Noachian Mars. In contrast to the carbon isotopes, the oxygen isotopic ratios ($^{18}O/^{16}O$) in the Martian atmosphere and water vapor are considered to be buffered by large O-reservoirs on Mars, such as the crustal rocks and the near-surface ice (Webster et al. 2013).

Although we have learned much from the study of Martian meteorites, retrieving the whole Mars history from current meteorite collections is highly challenging, especially regarding the evolution of the early environment (Noachian to Hesperian), mainly because of the following difficulties. The first concern is possible contamination of the Martian rocks by terrestrial water, air and/or organic matter. Most Martian meteorites land resided on terrestrial hot deserts or Antarctic ice and weather for a long time before they are finally collected. Even 'fall meteorites' (those collected shortly after their arrival to Earth) may have been affected by the terrestrial surroundings within a short time (Stephant et al. 2018). Contamination would also occur during laboratory processing (although this can be reduced by recent technical improvements).

Second, and possibly fatal, is the sampling bias of Martian meteorites. As noted above, most Martian meteorites are middle-to-late Amazonian igneous rocks (Nyquist et al. 2001; McSween and McLennan 2014). The only one Noachian igneous rock (i.e., ALH 84001; Mittlefehldt 1994; Lapen et al. 2010) and one Noachian clast-bearing breccia (i.e., the NWA 7034 series; Agee et al. 2013; Humayun et al. 2013) were found. The latter suffered severe metamorphism during Amazonian age. No meteorite contains Hesperian-aged materials. The cause of such sampling bias has been unsolved, although severe shock effects during meteoritic ejection (with the peak shock pressures up to ~ 15–45 GPa; Nyquist et al. 2001) may be a dominant reason. In order to escape from the Martian gravity and reach Earth, the rock had to be accelerated to > ~ 5 km/s probably by a heavy impact. In such ejecta, fragile sedimentary materials including the aqueous alteration phases (e.g., clays, carbonates, sulfates, and chlorites) and the organic compounds should have been broken and lost before arriving to Earth as "meteorite". On the other hand, ejecta with much lower velocity (i.e., lower shock pressure) can reach to the surface of Phobos (Ramsley and Head 2013; Nayak et al. 2016; Hyodo et al. 2019). This suggests that the Martian sedimentary materials, which are quite important for the Mars surface history, but rarely found in the Martian meteorites, have been accumulated and preserved on the surface of Phobos (Usui et al. 2020).

The recent calculation estimates that at least > 340 ppm of Martian ejecta is mixed in with Phobos regolith (Hyodo et al. 2019), suggesting that more than ~ 30 grains out of the 10-g Phobos sample collected by the MMX sampling system will have a 'Martian' origin. As the Martian ejecta can be delivered to Phobos by numerous random impacts, the obtained Martian grains may represent various geological eras on Mars and cover the whole evolution history. These Martian grains in the regolith on Phobos with a typical grain diameter of 300 μm is expected to contain more than one "chronometer" mineral (e.g., zircon, baddeleyite, or Ca-phosphate for U–Pb dating) in the case that the typical size (< 30 μm) and abundance (~ 0.1–1%) of chronometer minerals are comparable to those of Martian meteorites (McSween 2015). The chronometer minerals record the timing of formation and/or metamorphism of the individual grains. Thus, ~ 30 Martian grains returned by MMX would provide a wealth of "time-resolved" information on the evolution of Martian surface environments because these grains would have been transported randomly from any of the seven geologic units. More importantly, this will enable us to obtain precise isotopic compositions of key volatiles

Fig. 1 A schematic view of QSO. The spacecraft is orbiting Mars near Phobos, but from Phobos it appears as if the spacecraft is orbiting Phobos

reviewed above (i.e., D/H, $\delta^{13}C$, $\delta^{15}N$ and noble isotopes) via in situ analyses of the individual grains.

The surface mineralogy and chemistry of Phobos depends on its origin (summarized by Usui et al. 2020). In the captured (D- or T-type) asteroid origin hypothesis (Murchie and Erard 1996), the endogenous regolith on Phobos may present chondritic chemistry and mineralogy, probably like those of carbonaceous chondrites. On the other hand, if Phobos had formed through a giant impact on early Mars instead (Rosenblatt et al. 2016; Hyodo et al. 2017), its regolith may originate in Martian interior rocks with high temperature–pressure phases and the bulk Martian chemistry. Whatever the origin of the endogenous materials on Phobos, however, the exogenous grains (i.e., the Martian ejecta on Phobos) can be clearly distinguished based on their mineralogy and chemistry and will be confirmed by analyses of stable isotopes, including O, Cr and Ti. Once the grain is recognized as 'Martian', a series of organic and inorganic analyses will be investigated on the individual grains, including the volatile isotopic compositions, the U–Pb and other radiometric chronology, remnant magnetization, as well as possible Martian biosignature. Further analytical strategies and expectations are provided by Fujiya et al. (this volume).

Mars observation by MMX
Orbit and observation window
MMX will travel in a cruising orbit to Mars for 1 year, observe Mars and its moons for 3 years from 2025 to 2028, and eventually bring back collected samples to the Earth after a 1-year journey. During most of its 3-year mission, MMX trajectory will be in Quasi-Satellite Orbit (QSO) around Phobos, which is very similar to Phobos orbit around Mars: nearly equatorial and circular, with

a period of 7h40′ and distance of about 9,376 km from the Mars center (about 6000 km from the Mars surface) (Fig. 1). The detailed descriptions of QSO orbits and definition of the mission phases can be found in the companion paper in this special issue. In operation on Mars Moon proximity, remote sensing for atmospheric phenomena and in situ measurement for atmosphere escaping are continuously conducted on QSOs as a home position throughout the mission from Mars Orbit Insertion (MOI) in Phase 0. After arrival on Phobos QSO on October 2025, the landing site selection and the touchdowns to Phobos surface have the first priority over all considerations during the first one-half years from October 2025 to July 2027 as defined in Phases 1, 2, and 3. Mars observation will be made during the first one-half of year without interfering with Phobos observations or its data transfer (e.g., while on the nightside of Phobos). In the latter half of the mission from August 2027 to September 2028 as defined in Phases 4 and 5, we will have much more time to focus on Mars observations. Especially, the transfer orbits during Deimos flyby in Phase 5 will allow to explore Mars' surface and atmosphere with a different perspective thanks to elliptic orbits that enable the time-resolution observation of larger area than in QSO thanks to the increase on distance and decrease on ground speed around apoapsis.

Mars observation by MMX from the Martian equatorial plane (inclination of $\sim 1°$) has several assets. This circular orbit is relatively close to Mars when comparing to the areostationary orbit. MMX orbital motion ($0.013°/s$ with the period of 7h40′) will be faster than the rotational period of Mars ($0.004°/s$). As a consequence, the difference of rotation rate drifts the subsatellite point around $0.009°/s$. In 7h40′, subsatellite point shifts $\sim 248°$ eastward. After three orbits of 7h40′ (~ 23 h), subsatellite point has shifted of $\sim 744° = 2 \times 360° + 24°$, so MMX is located above a longitude 24° east of that three orbits ago. Quasi-areostationary orbiters are innovative platforms for space-born Mars science, as has been geostationary satellite imagery which revolutionized Earth weather forecasting from 1970s. The first equatorial orbiters will blaze a trail for the continuous remote sensing of the Martian atmosphere. Remote sensing from high orbit will enable to work in conjunction with satellites in polar or eccentric low-altitude orbits, which provide truly global coverage and synergistic perspective. From the equatorial plane, it is however noted that the apparent visible disk of Mars takes up a field of view of about $\sim 43°$. The coverage reaches up to approximately 68° latitude. In addition, the equatorial orbit of MMX will essentially increase opportunities to directly measure the low-energy outflow of ionospheric ions from Mars in the inner magnetosheath, which has been poorly understood so far.
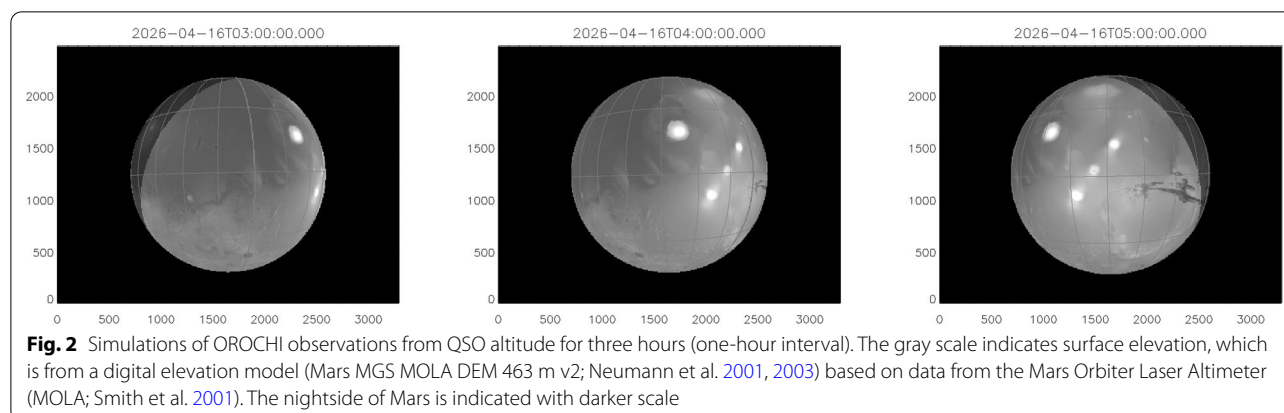
Instruments

The mass spectrum analyzer (MSA) is a scientific instrument onboard the MMX spacecraft, which consists of an ion energy mass spectrometer and two magnetometers (Yokota et al. 2021). The ion spectrometer measures distribution functions of low-energy (< 10 s keV) ions and their mass/charge distributions using a top-hat electrostatic energy analysis and a linear-electric-field time-of-flight mass analysis. The fluxgate magnetometers measure the vector magnetic field of the solar wind, which is occasionally perturbed by Mars and possibly Phobos in their neighborhood. The MSA experiment is designed to perform in situ observations of secondary ions emitted from Phobos, water ions generated from the Phobos torus if exists, and escaping ions from the Martian atmosphere with monitoring the solar wind. The MSA is developed based on the techniques used for previous space plasma missions such as KAGUYA (Yokota et al. 2005; Saito et al. 2010; Tsunakawa et al. 2010), ARASE (Yokota et al. 2017; Asamura et al. 2018; Matsuoka et al. 2018), Bepi-Colombo/MIO (Delcourt et al. 2016; Saito et al. 2020). Thus, the performance is similar to that of typical space plasma instruments except the mass resolution of $M/\Delta M \sim 100$, because the MSA will measure heavy ions and their isotopes coming from the Martian atmosphere to estimate the amount of the atmospheric escape. MMX will be located in the Mars shadow (eclipse) at approximately half of the year. In these periods, MMX will measure escaping ions in the magnetotail. In other periods, MMX will observe the solar wind. Seasonal variation of the MMX orbit with respect to the magnetotail can allow us to observe the longitudinal–latitudinal structure of escaping ions at 6000 km distance from Mars.

Since the MSA ion analyzer has a hemispherical field-of-view, solar wind ions can be continuously caught at the same time in many cases of the MMX nominal observation. Escaping ions from the Martian atmosphere will be measured when the spacecraft is in the Martian tail region together with Phobos. Only to observe secondary ions emitted from Phobos, the surrounding electric field must direct from Phobos to the spacecraft, because the ions with initial energies of ~ 0 eV travel along the electric field to the spacecraft.

Optical radiometer composed of chromatic imagers (OROCHI) is designed for capturing spectral features of Phobos from ultraviolet to near-infrared wavelengths with 7 wide-angle bandpass imagers and 1 panchromatic imager. Detailed information of design and performance of OROCHI is introduced in Kameda et al. (2021).

The field of view (FOV) of each imager is > 1 rad and the instantaneous FOV (iFOV) is 0.4 milli-radian. Figure 2 shows how Mars will be observed in the OROCHI's FOV. Because of the wide FOV, OROCHI can capture

Ogohara *et al. Earth, Planets and Space*   (2022) 74:1

Page 15 of 32

Fig. 2 Simulations of OROCHI observations from QSO altitude for three hours (one-hour interval). The gray scale indicates surface elevation, which is from a digital elevation model (Mars MGS MOLA DEM 463 m v2; Neumann et al. 2001, 2003) based on data from the Mars Orbiter Laser Altimeter (MOLA; Smith et al. 2001). The nightside of Mars is indicated with darker scale

whole disk of Mars in its FOV from the Phobos altitude with the pixel resolution of 2.4 km.

Since the orbit of MMX is similar to the Phobos orbit (see "Orbit and observation window" section), which is almost a circular orbit around Mars, OROCHI will observe Mars from almost same altitude (~6000 km), and thus it will provide images with a stable spatial resolution. Besides, OROCHI can monitor a specific region for more than 3 h with 2.4 km/pixel resolution and an interval of 15 min. This will give critical information for understanding how local/regional dust storms develop. The dataset from OROCHI is similar to those from a geostationary weather satellite whose spatial and temporal resolution are the order of 1 km and 10 min, respectively. Also, thanks to its wide FOV, OROCHI can observe a wide range of local time from morning to evening in one observation. It will also give a lot of information about local time dependence or morning–evening symmetry/asymmetry.

The center wavelengths of the OROCHI bandpass filters are 390 nm, 480 nm, 550 nm, 650 nm, 730 nm, 860 nm, and 950 nm, and designed signal-to-noise (S/N) ratio for spectral analysis (i.e., band ratios) is 100 (Kameda et al. 2021). For Mars observation, the blue and red bands will be mainly used for monitoring atmospheric dynamics. Dust and water ice clouds can be roughly distinguished based on a difference in brightness between the two bands. The high SN ratio is enough to resolve the difference in the photometrical properties between dust and water ice (c.f. Bell et al. 2009). The near-infrared band (950 nm) will be also important to connect the OROCHI images and MIRS data since the wavelength is commonly used by both instruments, then more detailed spectral analysis will be possible.
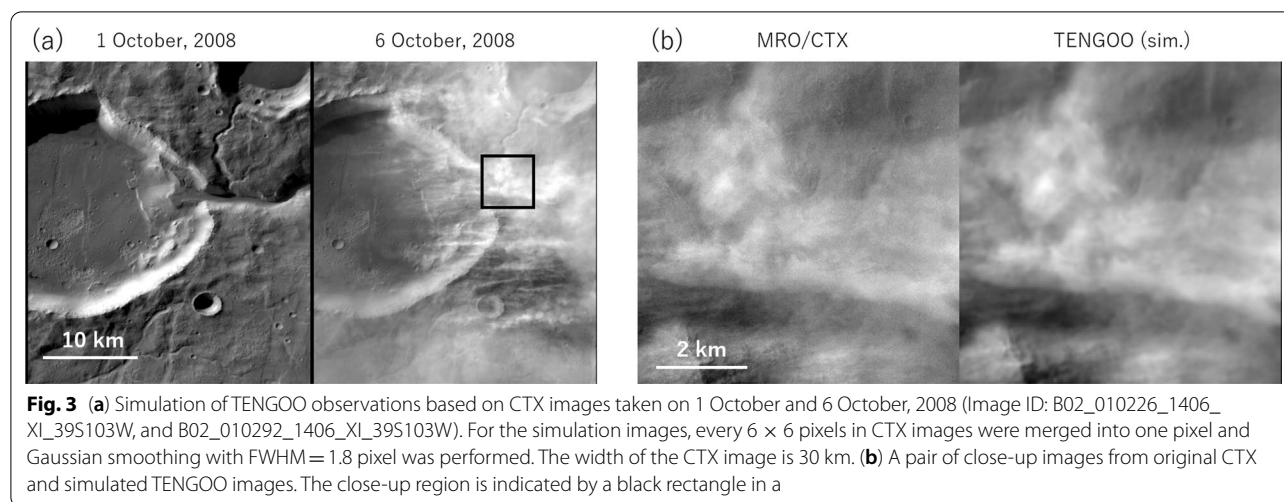
Telescopic Nadir imager for GeOmOrphology (TEN-GOO) is a panchromatic (370–850 nm) imager with a quite high spatial resolution, < 6 μ-radian/pixel, which is 60 times higher than that for OROCHI. The high spatial resolution allows to observe the Martian surface with a resolution of 35 m/pixel from the altitude of Phobos, thus we can analyze sub-km scale atmospheric phenomena from TENGOO images. TENGOO's FOV is $0.82 \times 1.1°$, which corresponds to 86.5×115.5 km region in one TENGOO FOV when observing Mars from the QSO.

Figure 3 shows examples of images that we expect TENGOO will take. The images were made from Context Camera (CTX) onboard Mars Reconnaissance Orbiter whose spatial resolution is 6 m/pixel (Malin et al. 2007). To simulate TENGOO observation from a CTX image, every 6×6 pixels of the CTX image are merged into one pixel and Gaussian smoothing is performed with full width at half-maximum (FWHM) = 1.8 pixel based on a high-resolution camera onboard Hayabusa-2 (Kameda et al. 2017). Even after the pixel merging, fine-scale dust streams can be clearly seen in the image (the event was introduced by Malin et al. 2009). Therefore, TENGOO is expected to resolve finer structures in dust storms and ice clouds with spatial scales of about 10 km. We may understand a short timescale variation of a local dust storm by sequential observations with TENGOO.

Same as OROCHI, the most significant advantage of TENGOO observation is that TENGOO can conduct a sequential observation for several hours which is critical for understanding short timescale atmospheric phenomena on Mars. Thanks to the high spatial resolution of TENGOO, we may track sub-km scale dust flows, and then we will be able to retrieve a local wind distribution in the FOV of TENGOO. TENGOO was originally designed to observe Phobos, not Mars. However, it allows us to make some significant observations described above. We plan to propose observations of Mars using TENGOO ("Observation campaign" section).

MMX InfraRed Spectrometer (MIRS) is a push-broom imaging spectrometer in the near-infrared spectral range (0.9 to 3.6 μm). MIRS detector is a 2D array providing image of a strip in one spatial direction with the spectrum

Fig. 3 (**a**) Simulation of TENGOO observations based on CTX images taken on 1 October and 6 October, 2008 (Image ID: B02_010226_1406_XI_39S103W, and B02_010292_1406_XI_39S103W). For the simulation images, every 6 × 6 pixels in CTX images were merged into one pixel and Gaussian smoothing with FWHM = 1.8 pixel was performed. The width of the CTX image is 30 km. (**b**) A pair of close-up images from original CTX and simulated TENGOO images. The close-up region is indicated by a black rectangle in a

of each point in the spectral direction. A second spatial direction is provided by the instrument line of sight in the along-track direction of MMX. MIRS FOV is ± 1.65° and while targeting a spatial resolution of 10 km on Mars, MIRS expected geometric resolution on Mars from Phobos orbit is ∼ 2 km so spatial binning can be implemented to increase signal-to-noise ratio and decrease data volume. MIRS has a spectral resolution of about 20 nm and a targeted signal-to-noise ratio above 100 for features of interest. Further detailed information on the instrument can be found in Barucci et al. (2021).

MMX quasi-circular orbit with a period of ∼ 7 h, will provide more than 3-h windows to MIRS. Different observation strategies will be possible to maximize either temporal or spatial coverage of MIRS monitoring of Martian atmosphere, from 30' time resolution observation of a limited zone to a complete coverage in a few orbits (see Barucci et al. 2021). MIRS will also perform limb observations to obtain information on Martian atmosphere at high vertical resolution.

MIRS observations will be used to constrain transport processes for dust and water in the Martian atmosphere, observations of the equatorial to mid-latitude distributions of dust storms, water ice clouds and water vapor. CO_2 (and thus pressure) will be monitored through CO_2 2.0 μm band. Water vapor will be monitored on a daily basis using its 2.6 μm band (Maltagliati et al. 2008) and water ice clouds through their spectral features between 0.9 and 3.6 μm (Vincendon et al. 2011). MIRS will be able to detect CO and O_2 with their 2.35-μm and 1.27-μm bands, respectively. MIRS will also provide monitoring of the atmospheric dust content and of water adsorbed in the surface regolith. Finally, in collaboration with the OROCHI and TENGOO instruments, it will also be

possible to investigate CO_2 clouds following the procedure proposed by Vincendon et al. (2011).

By providing long-term monitoring of multiple Martian atmosphere constituents, MIRS observations, together with the ones from MSA, OROCHI and TENGOO, will help better understand the interdependencies of these species and their roles in the Martian water, CO_2 and dust cycles.

Baseline operation
Once inserted into QSO, the spacecraft will spend most of its time in this QSO. Therefore, the basic operation for Mars observation should be planned for the period that the spacecraft stays in the QSO before and after touchdowns on Phobos. Basically, when the spacecraft stays on the dayside of Mars and the nightside of Phobos, we can allocate observation time to Mars. This is because most of the time on the dayside of Phobos will be spent on remote-sensing observation of Phobos, and our instruments are not sensitive enough to observe the night-side of Mars. The orbital period of Phobos is approximately 7 h and 40 min (0.31 sols, mean solar day on Mars). Thus, while the spacecraft is in the QSO, it enters the day and nightsides of Mars every 3 h and 50 min. On the other hand, the pseudo-orbital period of the spacecraft around Phobos depends on the mean distance between the spacecraft and the surface of Phobos. It is about a month when the spacecraft is in orbit at a distance of 100 to 200 km from the Phobos surface, called QSO-H. It is roughly four (Earth) days in orbit at a distance of 50–90 km, called QSO-M. Finally, it is roughly 12 h in orbit at a distance of 30 to 50 km from the Phobos surface, QSO-L. Figure 4 shows the case of QSO-H. The period of the Phobos dayside where Mars is not observable lasts for half a month, followed by the period

Fig. 4 Time series of the sub-spacecraft points on Phobos and Mars at hourly intervals in the case of QSO-H. (**a**) Time series of Phobos local time of the sub-spacecraft (sub-SC) point on Phobos for one month. The day and night-sides of Phobos are indicated by small dots and crosses, respectively. (**b**) Time series of Mars local time of the sub-SC point on Mars for the last 5 days of the month. The day and night-sides of Mars are indicated by crosses and small dots, respectively. (**c**) Time series of longitude of the sub-SC points on Mars for the last 5 days of the month. Sub-SC points on Mars are indicated by crosses when the spacecraft is on the dayside of Mars and the nightside of Phobos

of Phobos nightside where Mars is observable for half a month as shown in Fig. 4a. Thus, only during the latter half of the month, observation time for Mars, the dayside of Mars, lasts 3.84 h every 7.67 h. The observable longitude range is shifted by about 120° to the west in each orbit around Mars. If we focus on a certain longitude, the next opportunity for continuous observation of that longitude will be one day later, and slightly earlier in local time (Fig. 4b, c). For example, if the sub-spacecraft point on Mars passes through 0°E at about 14:30LT, we can observe 0°E at about 11:30LT the next day. Figure 5 shows the case of QSO-M. The dayside of Mars is observable for 3.84 h every 7.67 h, the same as QSO-H, but the nightside of Phobos where Mars is observable lasts for 51 h every 102 h, overlapping with series of the day and nightsides of Mars. The observable longitude range will be shifted by about 120° to the west in each orbit around Mars, as in the case of QSO-H (Fig. 5c). Tendencies of the longitude and local time of the sub-spacecraft point are the same as in the case of QSO-H. The difference from the case of QSO-H is that the spacecraft enters the dayside of Phobos after about 2 days (Fig. 5c). It means that we will not be able to observe Mars. On QSO-L, the nightside of Phobos where Mars is observable lasts for 12 h every day. The total time to observe Mars within a given period

does not change for the three types of QSOs. For example, the total time that we can observe Mars in a month is about 180 h, quarter of a month.

Regardless of the type of QSO that the spacecraft stays in, the continuous observation time of 3 h 50 min remains the same. During this time, OROCHI continues to acquire a multi-colored full-disk image every 15 min. High temporal resolution observations of terrestrial dust events in the Middle East by the Spinning Enhanced Visible and Infrared Imager (SEVIRI) onboard Meteosat Second Generation (MSG) show that the number of dust events detected at 30-min intervals is clearly lower than that at 15-min intervals, especially during the summer months (Hennen et al. 2019). This is expected to enable us to monitor in detail the development of small-scale dust events over a wide area in low and mid-latitudes. The MIRS also continues to acquire several stripes with all the wavelengths during the observation time of 3 h 50 min.

The MMX is a three-axis stabilized spacecraft with a high gain antenna (HGA) fixed on the side (+X plane), and a medium gain antenna (MGA). As the HGA has a radiation pattern with a narrow beam width, the HGA boresight direction is precisely controlled toward the Earth for communications, while MGA takes advantage

Fig. 5 The same figure as Fig. 4 except that it is the case of QSO-M
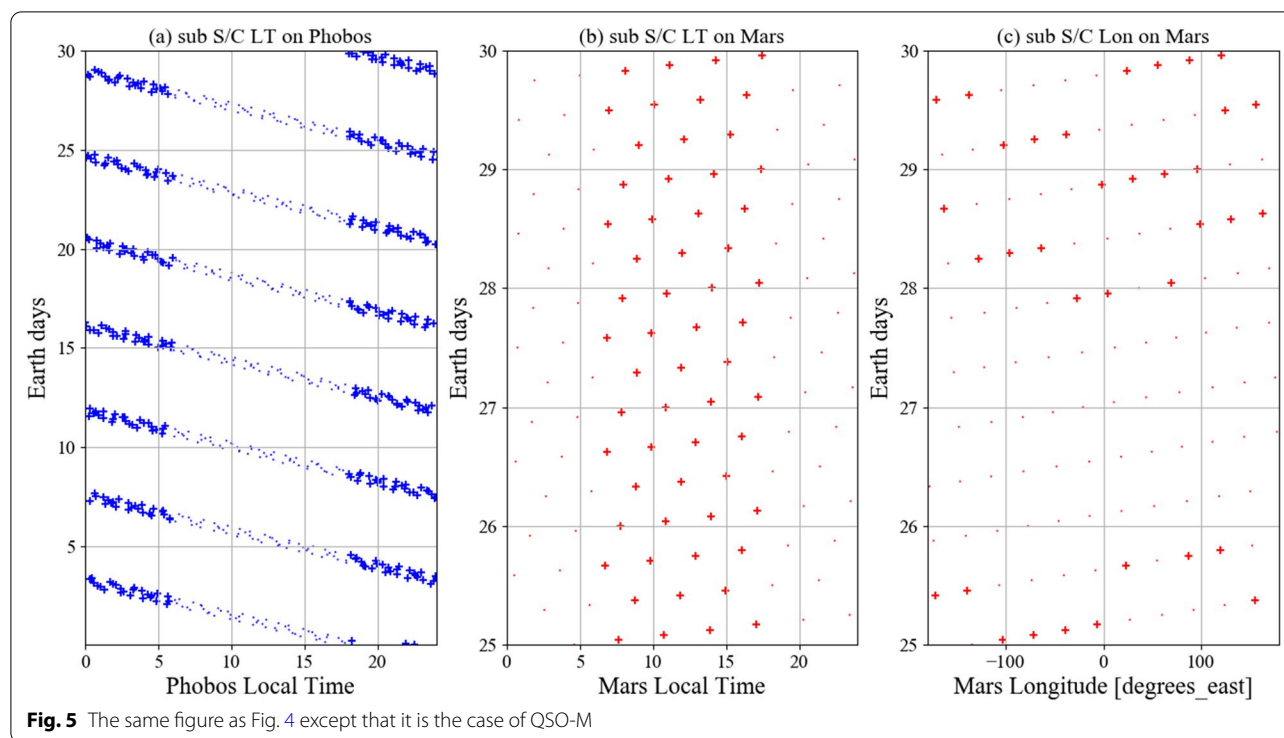
of the flexibility of the spacecraft's attitude and orientation control. In the nadir observation mode for atmospheric remote sensing, the -Z-axis boresighted along the viewing axes of the optical instruments is maintained towards the center of Mars (Fig. 1). Orientation is a spacecraft resource that has to be shared with Phobos observations. The slew maneuver from one orientation to another is required in order to switch between Mars observation and Phobos observation during QSOs. The spacecraft's slewing capabilities will also be used during observations of Mars in order to maximize the coverage of the MIRS on Mars disk, in combination with its scan mirror. The MIRS scans the area of interest from low to mid-latitudes within an hour. Along-track and cross-track scans are done by the MIRS's scan mirror and the maneuver of the spacecraft, respectively. We are also considering extending the observable latitudinal range by increasing the scan speed of the mirror while maintaining the temporal resolution, although the spatial resolution will be reduced. In any case, MIRS provides hourly horizontal distributions of quantities important to Martian meteorology around the area of interest, such as the amount of water vapor and dust.

Observation campaign

The basic operations described in the previous subsection alone can produce significant results. During the baseline operation, however, the optical instruments

are basically either pointing at the center of Mars or scanning in the cross-track/along-track directions. This means that the east and west Martian limbs are not in the field of view of the instruments other than OROCHI. We plan to conduct several limb observation campaigns, using MIRS, which will allow us to observe the limb over a wide latitudinal range within an hour, and to obtain vertical profiles of dust, water vapor, ice clouds, and dayglow/nightglow, etc. (e.g., Vasilyev et al. 2009). Sánchez-Lavega et al. (2018) reported the temporal variation of detached clouds and dust seen in limb observations by Visual Monitoring Camera (VMC) onboard MEX. The vertical resolution of VMC depends on the altitude of MEX above the Mars surface and ranged from 350 m to 8.5 km in their cases. If TENGOO is pointed at the limb at a high frequency (e.g., 1 image/min) by the maneuver of the spacecraft, it may be possible to track the temporal changes in the vertical distribution of dust and clouds with much higher vertical resolution than that of VMC. And if this coincides with the MIRS limb observations, it will be easier to distinguish between dust and clouds. In this limb mode, the -Z-axis of the spacecraft is pointed in a precalculated orientation so that the instruments scan across the limb. The slit and scan mirror of MIRS, and CCD imagery of the TENGOO may be positioned parallel to the limb. In any cases of the limb observations, the FOV of OROCHI is so wide that OROCHI can

observe most parts of the Mars disk even if the other two instruments are pointing at the limb.

Another target for campaign observations is atmospheric phenomena that are already known to occur in a particular region. For example, ice clouds are frequently observed around the high mountains (Wang and Ingersoll 2002), and numerical simulations show that they are formed by upslope winds (Spiga and Forget 2009). The spatial scale of these ice clouds is on the order of 10 to 100 km, and their formation should be closely linked to diurnal phenomena (Wilson et al. 2007). Dust haze inside the Valles Marineris has been observed by MEX (Inada et al. 2008). The Valles Marineris is also the site of "puffy" dust storms defined by Kulowski et al. (2017). These dust events are mesoscale phenomena and so their development should be controlled to some extent by the diurnal variation. Ogohara and Satomura (2011) listed several other areas (the Acidalia Planitia, the Arabia Terra, the east of the Elysium Mons, and the Sirenum-Aonia region) where dust haze tends to spread in addition to the mountainous areas and the Valles Mariners suggested. The formation, transport and dissipation of clouds and dust events can be observed in detail with high temporal resolution if MIRS and TENGOO are pointed at these regions. However, whether we can really

point the spacecraft freely to those areas depends largely on the thermal conditions and communication rates of the spacecraft at the time. Frequent observation of high-resolution images means an increase in the amount of data. Therefore, considering such external conditions, the feasibility of campaign observations, including when they are feasible, will be examined. We are currently investigating whether there are any other important observations other than the two campaign observations mentioned above. Compromises and a use case of various observation modes for atmospheric remote sensing will be also investigated.

Synergy with other missions

The recent years have seen a renewed interest whole throughout the Martian atmosphere, thanks to the aggressive explorations by the MRO, MEX, Curiosity rover, MAVEN and TGO missions, etc.; we now appreciate that it is considerably mutually coupled system of the surface, lower and upper atmospheres, and the surrounding space environment than previous expected (e.g., Nakagawa 2019). However, their spatial coverage and temporal resolution are often strongly limited by the FOV of the instrument and the orbit of the spacecraft. Figure 6 is a schematic view showing the orbits of the
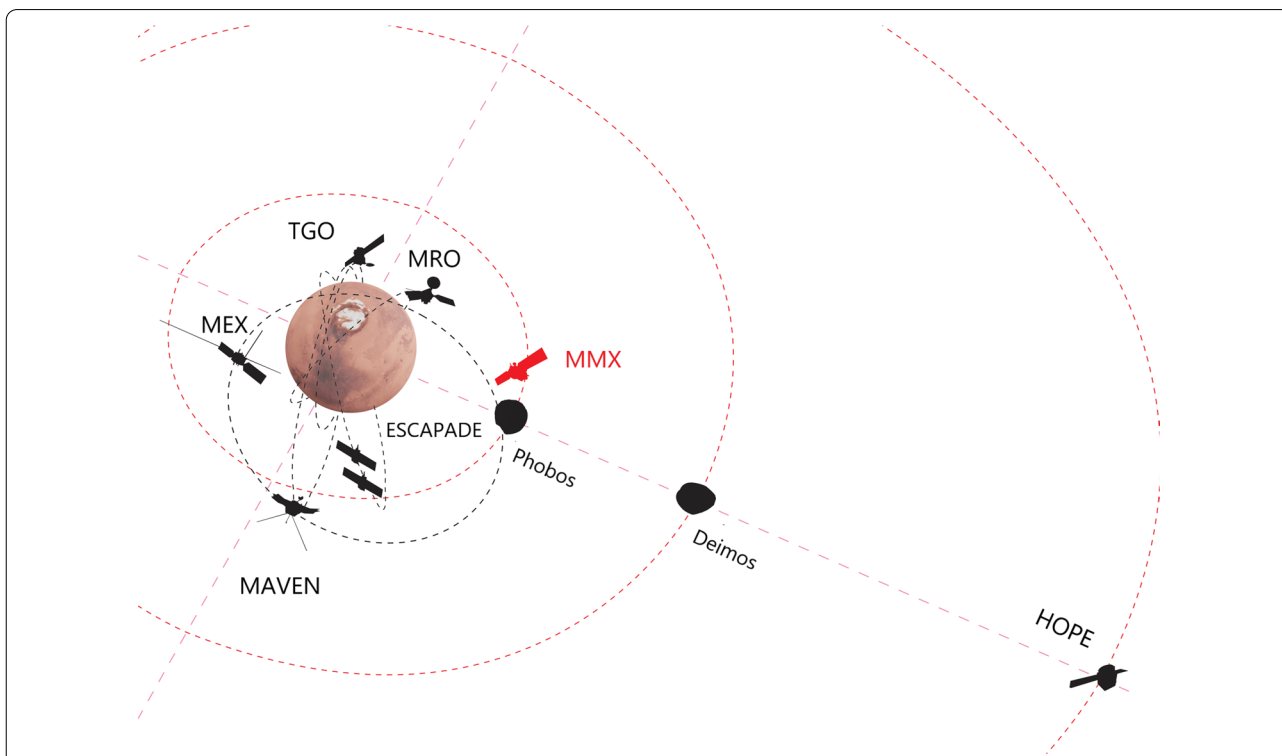

Fig. 6 A schematic view of the orbits of the ongoing and future missions. The orbit of MEX appears in this figure to be similar to that of MMX, but in fact an elliptical polar orbit with an apoapsis in the southern hemisphere is intended
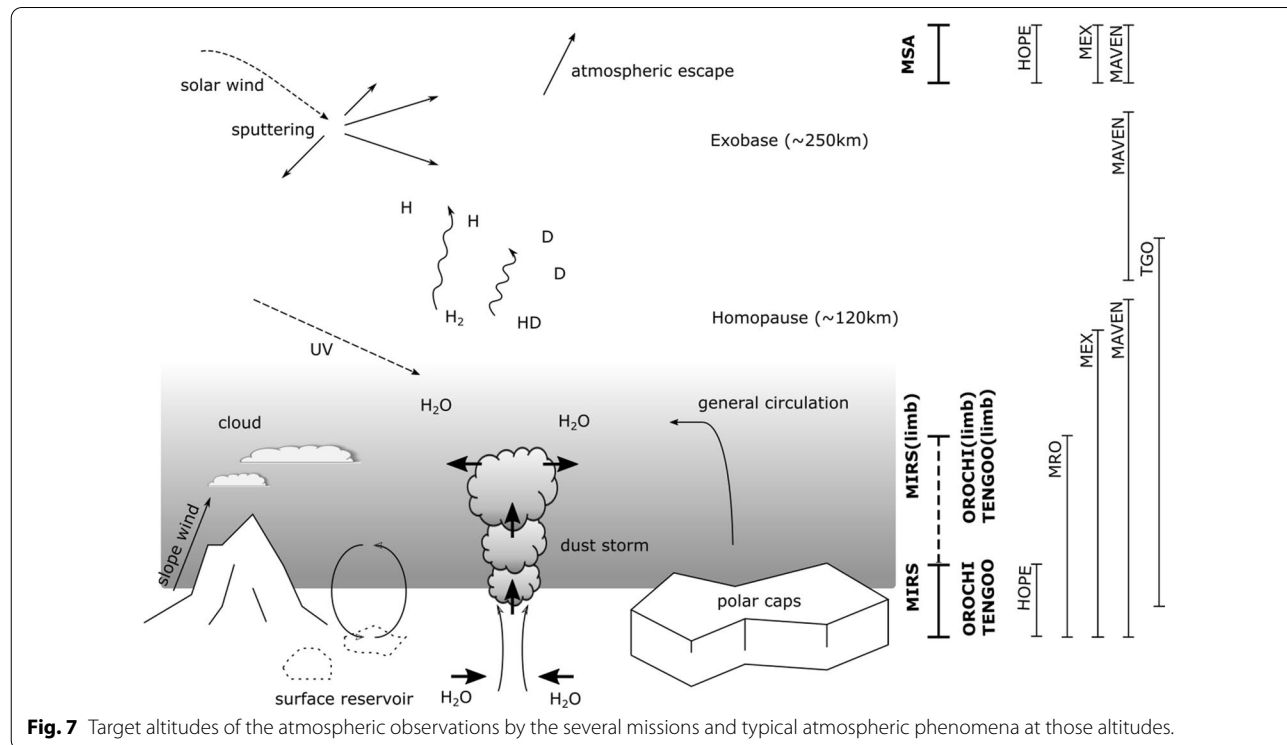
ongoing and future spacecrafts. Orbit is closely linked to the spatial coverage of a single observation and the temporal resolution. MMX's trajectory, which is quite different from other missions, means that it will produce a completely different type of dataset in terms of temporal resolution and observational coverage.

In order to complete our understanding of atmospheric mutual coupling system, the monitoring capability throughout the atmosphere from near-surface to the space is of importance. Figure 7 shows target altitudes of several missions including MMX and atmospheric phenomena at those altitudes. MMX covers the lowest and highest altitudes, while the other polar-orbiting satellites observe the altitudes in between, including the near-surface atmosphere. MAVEN can observe the widest range of observational altitudes from the surface to space. The limited target altitude of MMX is due to the fact that it is designed to monitor atmospheric phenomena in the lower atmosphere, which has small spatial scales and large temporal variations. Therefore, MMX and these missions are highly complementary, both in terms of the time resolution and spatial coverage derived from the orbit, and in terms of observation altitude.

Overview of each mission

Mars Express represents the first attempt of Europe to visit another planet in the Solar System (Chicarro et al. 2004). Mars Express (MEX) has remained in orbit around

Mars since the end of 2003, delivering a continuous and diverse survey of Mars, monitoring all the components of the Martian system from the subsurface to the exosphere, including the surface, the neutral atmosphere, as well as the magnetosphere. When the MMX mission will be reaching its destination, MEX will have spent more than 20 years in orbit and should still be in good health to join MMX in its observing campaign. MEX has set the path for helping MMX prepare its future exploration, with its recurrent observations of the Martian moons, leading to a better characterization of Phobos properties in particular (Witasse et al. 2014). With the Observatoire pour la Minéralogie, l'Eau, les Glaces et l'Activité (OMEGA, a hyperspectral imager, Bibring et al. 2004) and the High-Resolution Stereo Camera (HRSC, Neukum et al. 2004), Mars Express will be able to assist and complement MMX MIRS, TENGOO and OROCHI in their imaging quest of Mars, Phobos and Deimos surfaces. All these instruments feature comparable characteristics, delivering images at a variety of wavelengths, from UV (> 390 nm) to infrared (< 5 μm), where surface and atmospheric components possess distinct imprints. However, the ~ 1-h temporal sampling of MMX will allow a systematic characterization of the diurnal cycle of the Martian atmosphere at any given place of the planet throughout the MMX mission lifetime, such thing that MEX could only tentatively address after years of observations with the Planetary Fourier Spectrometer (PFS, Giuranna et al.

Fig. 7 Target altitudes of the atmospheric observations by the several missions and typical atmospheric phenomena at those altitudes.

Ogohara *et al. Earth, Planets and Space*   (2022) 74:1

Page 21 of 32

2021) or with the Spectroscopy for Investigation of Characteristics of the Atmosphere of Mars (SPICAM, Montmessin et al. 2017). Combining MMX capability with, e.g., recurrent solar occultations by SPICAM, it should be possible to establish a better understanding of the partitioning of water vapor between the near-surface accessed by MMX quasi-ubiquitously and the atmosphere above where solar occultations provide a high vertical resolution. While MMX has no capability to directly extract temperature profiles, PFS and the Mars Radio Science experiment (MaRS, Hinson et al. 2019) will be able to fill partially this gap up to > 40 km of altitude, but only for a small fraction of the maps produced by MMX. Between MMX/MSA, MEX/MaRS and The Analyser of Space Plasma and Energetic Atoms (ASPERA), and MAVEN (Jakosky et al. 2015), three spacecrafts will sample simultaneously the Martian magnetosphere at three different locations for the first time, enhancing the coverage in the characterization of the ionized atmosphere, providing unique insights in the escaping mechanisms prevailing on the planet. In particular, the permanent position of MMX at a distance of Mars where it will essentially sample the solar winds will make MMX extremely complementary to MEX whose elliptical orbit as MEX is capable to penetrate the Martian atmosphere down to ~ 300 km far from the surface at periapsis, with an apoapsis located at ~ 10,000 km.

The ExoMars Trace Gas Orbiter is an European Space Agency (ESA)/ROSCOSMOS mission dedicated to the investigation of the Martian atmospheric trace gases and their sources, and how the water and the geochemical environment varies, i.e., by characterizing their distribution in the atmosphere, on and near the surface or as a function of depth in the shallow subsurface (Vago et al. 2015). TGO was launched in March 2016, and started its science phase in April 2018. With its near-circular orbit (eccentricity of 0.0069), varying between 380 and 430 km above the planet's surface, with an inclination of 74°, the ground track repeats after 30 sols with one orbital period being approximately 2 h long (12 orbits in one sol). This orbit provides optimum coverage of the surface and solar occultation possibilities for the science instruments, while still allowing the spacecraft to relay data from the different assets now on the planet, as well as from future landers and rovers. EMTGO comprises four instruments: CASSIS, Colour and Stereo Surface Imaging System (Thomas et al. 2017), FREND, Fine Resolution Epithermal Neutron Detector (Mitrofanov et al. 2018), and two spectrometers' suites, ACS (Atmospheric Chemistry Suite, Korablev et al. 2018) and NOMAD (Nadir and Occultation for MArs Discovery, Vandaele et al. 2018). The two missions will be complimentary in that MMX will provide the global context to TGO, which

has a smaller field of view but can still observe vertical distribution of dust, water vapor, and other trace gases with high accuracy by solar occultation technique. The high temporal resolution observations by OROCHI and MIRS can fill in the gaps of observations by TGO. This will be of particular importance to understand the impact of dust storms, global or regional, on the transport of trace gases within the atmosphere. On the other hand, NOMAD and ACS can also derive the vertical distributions of the atmospheric temperature, while MIRS will not be able to measure them accurately. So, TGO can contribute to understanding the dynamics controlling the transport of the tracers that will be discovered by MMX, perhaps through numerical simulations and data assimilation of the temperature distributions. Also direct comparison and mutual validation will be possible between instruments on both missions, as for example between the NOMAD and MIRS nadir observations, or between the cameras.

Al Amal ('Hope' in Arabic), also known as the Emirates Mars Mission (EMM), was successfully launched to Mars from the Tanegashima Space Center in Japan on 20 July, 2020, the 51st anniversary of the Apollo 11 Moon landing. EMM will make measurements relevant for understanding energy transport in the Martian atmosphere, both within the lower atmosphere (as a function of local time, geographic location, and season) and between the lower and upper atmosphere (Sharaf et al. 2020). EMM carries three science instruments: the Emirates Mars Infrared Spectrometer (EMIRS, 6–40 microns), a multiwavelength 12-megapixel visible and near-UV imager (Emirates eXploration Imager, EXI), and an ultraviolet spectrometer (100–170 nm). The orbital inclination of the spacecraft is low (~ 25°) and the orbital period is large (~ 55 h), so that EMM's measurements will typically be global (e.g., EXI's images will contain the full disk of Mars). This orbit will enable EMM to measure all longitudes on Mars at all times of day every ~ 10 days—something that has not been possible with previous Mars spacecraft. The nominal mission for EMM is one Mars year (spring 2021-spring 2023), with a possibility for mission extension for an additional Mars year. Thus, it is unlikely that EMM and MMX will overlap as active missions at Mars. However, the datasets from the two missions will be complementary, and therefore the EMM observations may help to inform the MMX observations. Both missions will investigate transport processes for water and dust in the lower atmosphere. The EMIRS can observe spatial distributions of the major tracers and temperature in the lower atmosphere although its spatial resolution on Mars is much lower than the MIRS onboard MMX. MIRS can monitor temporal variations of the much finer structures of the tracers than

the EMIRS's spatial resolution while it will not be able to measure temperature accurately near the Mars surface. Both missions will also investigate escape of the Martian atmosphere to space. EMM can observe neutral molecules escaping from Mars, while MSA onboard MMX can detect escaping ions.

MRO, which was launched on August 2005, has observed the Martian atmosphere for about 15 years (Zurek and Smrekar 2007). Its orbit is the sun-synchronous polar orbit and therefore it can observe 12–13 longitudes for each latitudinal band for one sol. The local time of observations will correspond to slightly after midnight and noon. This type of orbit is suitable for monitoring diurnal to seasonal variations of weather systems in all latitudes. Observations of the day and nightsides of Mars at several longitudes every sol enable us to derive the meridional distributions of zonal mean of observed variables (e.g., the atmospheric temperature). Mars Climate Sounder (MCS) has quantified the vertical and horizontal variations of water vapor, dust, and the atmospheric temperature (Kleinböhl et al. 2009) on the dayside and nightside of Mars and the database that has been accumulated since the MOI reveals their seasonal and annual changes. Mars Color Imager (MARCI, Bell et al. 2009) is a push-bloom camera with a wide longitudinal FOV and can scan Mars in the latitudinal direction following the satellite's orbital motion. Accordingly, MARCI can cover the whole of Mars surface in one sol. However, if we focus on a particular region, the time resolution of observations of the region is worse than half a sol except the polar regions. MARCI that uses visible wavelengths filters can take only one image of the regions every sol. MCS can observed the nightside of Mars, but the longitudinal resolution of the observations is low due to its narrow FOV and limb-viewing operation. Therefore, the instruments onboard MRO cannot monitor rapid variations of fine structures in the spatial distributions of the tracers with shorter time-scales than one sol and smaller horizontal scales than the synoptic scale. Although MMX cannot observe the nightside of Mars, it fills in the gaps between MRO observations and reveals the continuous variations in the fine distribution of water vapor and dust.

MAVEN is a NASA Mars-orbiting spacecraft mission dedicated to investigating the upper atmosphere and plasma environment around Mars in order to determine the role of the atmospheric escape to space has played in altering the Martian climate over the planet's history (Jakosky et al. 2015). MAVEN was launched in November 2013 and entered into orbit around Mars in September 2014. MAVEN carries 9 science instruments to measure the solar and solar wind drivers of escape, the upper atmospheric reservoirs for escape, and the

escape processes and rates. These measurements have also enabled to determine that the atmospheric escape has played an important role in Martian climate evolution, such that the atmospheric escape removed half a bar or more of CO_2 from the atmosphere over Martian history (Jakosky et al. 2017). The MAVEN instruments consist of both in situ particle and field detectors and a remote sensing package. Having a mission dedicated to a single science goal making coordinated observations has enabled a number of new or unexpected discoveries, including diffuse aurorae over the entire Martian disk (Schneider et al. 2015), the response of the Martian upper atmosphere to both dust storms and solar storms (e.g., Lee et al. 2020, and the complex magnetic configuration near Mars driven by crustal magnetic fields (e.g., Xu et al. 2017, DiBraccio et al. 2017.) MAVEN's instruments are currently all working well, and the mission is expected to last until 2030. Therefore, the MMX MSA instrument and MAVEN could potentially make simultaneous observations of the Martian magnetosphere and the solar wind. If the MEX mission is also extended, three multi-point measurements of MEX, MAVEN and MMX will strongly help distinguish between temporal and spatial variabilities of the solar wind-driven magnetospheric and ion escape processes at Mars.

ESCAPADE (ESCape and Plasma Acceleration and Dynamics Explorers) is a planned twin-spacecraft mission (in the preliminary design phase under the NASA's SIMPLEX-II program as of this writing) that will measure charged particles and magnetic fields around Mars. Ion and magnetic field data provided by MSA on MMX will be highly complementary to ESCAPADE (and the currently operating MAVEN and MEx missions, if extended) in multiple ways. First, the high mass resolution (M/dM ~ 100) of MSA complements other suprathermal ion instruments generally with lower mass resolutions by providing detailed information on ion composition and even on isotopes. Second, the MMX's nominal quasi-satellite orbit provides an equatorial, nearly circular orbit around Mars, enabling regular in situ sampling of the solar wind and magnetotail plasma every orbit, provided that the MSA's 2π sr field of view is oriented properly. Around the Phobos distance, MMX is expected to be located in the upstream solar wind for roughly half of the orbit around Mars under nominal solar wind conditions (e.g., Trotignon et al. 2006). The regular solar wind coverage is particularly valuable for other spacecraft in highly inclined, elliptical orbits with gradual precession of periapsis because they typically lose the solar wind coverage for a long duration once they are in an orbital configuration unfavorable for solar wind measurements. Finally, the addition of MSA data will augment the multi-spacecraft science originally envisioned by ESCAPADE.

If simultaneous observations by MMX and ESCAPADE are realized along with extended operation of MAVEN and MEX, there may possibly be 5 spacecraft with plasma instrumentation orbiting Mars. This will be an unprecedented opportunity for a rich variety of multi-point analyses on the highly dynamic and complex magnetosphere of Mars and planetary ions escaping through it. These analyses include, but are not limited to: (i) distinguishing spatial from temporal variations; (ii) simultaneous observations of drivers and responses, thereby monitoring time evolution of the system during solar transients, and (iii) timing analysis between multiple locations, thereby determining direction and speed of perturbations propagating through the system.

Synergy for each science theme

The study on the paleo-environment of Mars using the Martian samples that MMX will bring back to Earth is expected to have synergy with MSR first and foremost. The NASA–ESA-led Mars Sample Return (MSR) and MMX missions are both planned for the 2020s. MSR will return samples back to the Earth in 2031 from the Perseverance rover landing site Jezero crater (Beaty et al. 2019), whereas MMX will return the Phobos regolith in 2029 (Kawakatsu et al. 2017; Kawakatsu 2018). MSR will provide a comprehensive dataset regarding the single location with the geologic context. At the same time, MMX will return Martian surface materials ejected from multiple unknown locations by numerous impact processes (Hyodo et al. 2019). Together MSR and MMX are the first-ever missions designed to collect material samples from the Mars system for analysis. Eventually, their complementary nature will address questions on the origin (e.g., source of building blocks of Mars), interior evolution (e.g., crust–mantle differentiation), geologic history (e.g., hydrologic cycles), and the potential biological activity (e.g., nature and extent of habitability and preservation of biosignatures/biomarkers).

In order to understand the drastic climate change on early Mars and the evolutionary history of the total amount of CO_2 and H_2O reservoirs in the Martian surface environment, we need to understand the escape rates of H, O, and C as a function of external drivers, such as solar radiation and solar wind, from the observations of atmospheric processes and near-space environment of present-day Mars. As reviewed in the "Atmospheric escape" section, acceleration mechanisms of cold planetary ions depend both on tailward distance from Mars and solar wind conditions (e.g., Nilsson et al. 2012; Inui et al. 2019). While MSA measurements at a fixed tailward distance will provide data to assess the effects of solar wind conditions, a synergy with other missions with multi-point measurements by MEX/ASPERA,

MAVEN/STATIC, and ESCAPADE at different distances from Mars will give an unprecedented opportunity to clarify the acceleration mechanisms and escape channels of cold ions from Mars. Especially, simultaneous multi-point measurements of atmospheric response to an extreme transient event, such as CME and CIR, could provide a deep insight of the global structure of vigorous escape processes in the ancient days. Another synergy with other missions regarding this science theme is simultaneous observations from the ground to space in order to understand a possible connection between the Martian atmosphere and atmospheric escape. Although OROCHI and MIRS onboard MMX provide the detailed global monitoring of water vapor and dust in the lower atmosphere, the vertical evolution of water vapor and dust into the upper atmosphere should be complemented by sensitive occultation observations by MEX, TGO, and MAVEN. Mutual system of the Martian atmosphere and high-speed transport of water from lower to upper atmosphere could be clarified only by such synergy.

One of our objectives is continuous monitoring of rapid transport processes controlled by atmospheric phenomena with fine structures as described in the above sections. Spatial and temporal data coverage of this type of observations is completely different from that of typical polar-orbiting spacecrafts. MMX can monitor the rapid development of dust storms and ice clouds and the deformation of distributions of water vapor with a temporal resolution less than one hour. However, it cannot observe variables included in the basic equations of the atmosphere (e.g., temperature or velocity). Accordingly, the behavior of dust storms and water vapor revealed by MMX cannot be interpreted from MMX observations alone. On the other hand, typical polar-orbiting satellites, such as MRO and TGO, cannot monitor the rapid development of dust storms and other phenomena sequentially, but MCS onboard MRO and the two instruments onboard TGO can observe the synoptic structure of the atmospheric temperature on a daily basis. Especially, MCS can measure the atmospheric temperature even at the nightside of Mars. Zonal mean temperature and anomalies from the zonal mean derived from such polar-orbiting satellites are crucial to understand mechanisms of the behavior of tracers observed by MMX because they enable us to infer distributions of horizontal winds that actually transport the tracers. Another synergy with other missions regarding these science themes is simultaneous observations of dust, ice clouds, and water vapor by spectrometers. MIRS has comparable characteristics with MEX/OMEGA and is a powerful instrument for observation of fine structures of water vapor. Although MIRS will continue to hourly scan several areas of Mars, observation time cannot be always

assigned to Mars (e.g., during the dayside of Phobos). Therefore, coordinated observations between MMX and MEX may be able to fill in the missing observation period of water vapor distribution. In addition, EMIRS onboard HOPE can always obtain the global tracer distribution. Although its spatial resolution is much lower than that of MIRS and OMEGA, it can monitor the global structure of the atmosphere, in which the water vapor distribution obtained by MIRS and OMEGA is embedded. Of course, the complementarity between MMX and MEX in being able to fill in missing observation periods is also the case with other instruments on other spacecraft; using MRO/MARCI and HOPE/EXI allows for more continuous observations than OROCHI alone.

Summary

The aims of MMX with respect to Mars system sciences are:

- Obtain new information on the history of the Martian surface environment,
- Advance our understanding of material transport processes in the Martian atmosphere affecting the transitions in the Martian climate.

There is a possibility that Martian ejecta are deposited on the surface of Phobos. Moreover, those ejecta do not need to be launched as fast as the Martian meteorites. Therefore, it is possible that they have not been much thermally metamorphosed and may retain information from various eras. It is expected that the Martian ejecta deposited on the Phobos surface can be brought back to Earth for analysis to understand the environment on the Martian surface at various eras.

The Martian surface environmental changes in the past are closely related to changes in the amount of the atmosphere (i.e., the surface pressure). There is a large uncertainty in estimation of the total amount of H_2O and CO_2 that have been lost from the Martian atmosphere to space in the past. Comprehensive measurements of oxygen-, carbon-, hydrogen-bearing ion species with high mass resolution of MSA at the Phobos orbit will provide crucial constraints on H_2O and CO_2 escape rates at present-day Mars and its extrapolation backward in time. MMX will frequently enter the shadows of Mars and Phobos as it will stay in the Phobos orbit. MSA observations at the fixed distance from Mars will provide a unique opportunity to assess the effects of solar wind conditions on the cold ion escape process through the Martian-induced magnetotail. Another strength of the planned atmospheric escape observations is coordination with observations of the lower atmosphere of Mars by MMX as well as synergy with MEX, TGO, EMM, MRO, MAVEN, and ESCAPADE observations. We can verify whether the ion outflows are correlated with initiations and developments of dust events and ice clouds.

The major difference between MMX observations of the Mars lower atmosphere and previous missions is that MMX continuously observes a wide area from the equatorial orbit with high temporal resolution. This will help to elucidate the fine structures of water vapor near the Martian surface which have been observed recently, the distribution of water vapor associated with dust events, and their temporal variations. The rapid development and dissipation of sub-mesoscale to mesoscale atmospheric phenomena cannot, in principle, be observed by conventional polar-orbiting satellites. However, considering that the fluctuation component with the largest amplitude near the Martian surface is the diurnal variation, weather satellite-like observations such as MMX are essential to understand the mechanism of such small-scale dust events and ice clouds and the efficient vertical transport of water vapor and dust to the upper atmosphere by them, which may have contributed to efficient escape of H_2O. MMX will monitor the fine structure of dust and water vapor in the lower atmosphere with high temporal resolution, and will also observe atmospheric escape. On the other hand, the other spacecrafts are mainly observing the Martian atmosphere between the two altitudes from polar orbits. MMX is highly complementary to them in that it fills a spatio-temporal gap that has not been observed so far.

Ogohara *et al. Earth, Planets and Space*   (2022) 74:1

Page 25 of 32

Authors' contributions

KO, HN, SA, TK, TU, NT, TI, FM, DB, AD, TG, TH, YH, MK, FL, RR, ES, KS, AS, ACV, and SY prepared the initial manuscript. KO, HN, SA, TK, TU, NT, TI, and FM contributed to the development of mission objectives, consideration of integrated operation plans, and analysis of temporal variations in instrument field of view and footprint. HI and ES brought important technical information on the spacecraft and instruments and helped plan the baseline observations. SY, AB, SK, TK, HN, TG, AD and ES contributed to the design and development of the instruments. All authors provided us with feedback. All authors read and approved the final manuscript.

Funding

Availability of data and materials

The actual SPICE kernel for the probe will be released when the spacecraft is launched and the mission is executed.

Declarations

Ethics approval and consent to participate

Not applicable.

Consent for publication

Not applicable.

Competing interests

The authors declare that they have no competing interests.

Author details

[1]Faculty of Science, Kyoto Sangyo University, Motoyama, Kamigamo, Kita-ku, Kyoto, Japan. [2]Graduate School of Science, Tohoku University, 6-3, Aram-aki-Aza-Aoba, Aoba-ku, Sendai, Miyagi, Japan. [3]LPAP, STAR Institute, Université de Liège, Allée du 6 août, 19C, 4000 Liège, Belgium. [4]Royal Belgian Institute for Space Aeronomy, 3 Avenue Circulaire, 1180 Brussels, Belgium. [5]Artificial Intelligence Research Center, National Institute of Advanced Industrial Science and Technology, 2-3-6, Aomi, Koto-ku, Tokyo, Japan. [6]Department of Solar System Sciences, Institute of Space and Astronautical Science, JAXA, 3-1-1 Yoshi-nodai, Sagamihara, Kanagawa 252-5210, Japan. [7]Graduate School of Frontier Sciences, The University of Tokyo, 5-1-5, Kashiwanoha, Kashiwa, Chiba 277-8561, Japan. [8]LATMOS/IPSL, CNRS, Sorbonne Université, UVSQ-UPSaclay, Guyancourt, France. [9]LASP/University of Colorado, Boulder, CO, USA. [10]LESIA, Observatoire de Paris, Université PSL, CNRS, Sorbonne Université, Université de Paris, 5 place Jules Janssen, 92195 Meudon, France. [11]Space Sciences Laboratory, University of California, Berkeley, 7 Gauss Way, Berkeley, CA 94720, USA. [12]Graduate School of Science, Kyoto University, Kitashirakawaoiwake-cho, Sakyo-ku, Kyoto 606-8502, Japan. [13]Research and Development Directo-rate, Japan Aerospace Exploration Agency, 3-1-1 Yoshinodai, Sagamihara, Kanagawa 252-5210, Japan. [14]Graduate School of Advanced Science and Engi-neering, Hiroshima University, 1-3-1 Kagamiyama, Higashihiroshima, Hiro-shima 739-8526, Japan. [15]LATMOS/CNRS, Sorbonne Université, UVSQ, Paris, France. [16]Earth-Life Science Institute, Tokyo Institute of Technology, 2-12-1, Tokyo 152–8550, Japan. [17]Space Science Institute, Boulder, CO, USA. [18]CNES, 18 avenue Edouard Belin, 31400 Toulouse, France. [19]Department of Earth and Planetary Science, Graduate School of Science, University of Tokyo, Hongo 7-3-1, Bunkyo-ku, Tokyo 113-0033, Japan. [20]Laboratoire de Météorologie Dynamique/Institut Pierre Simon Laplace (LMD/IPSL), Sorbonne Université, Centre National de la Recherche Scientifique (CNRS), École Polytechnique, École Normale Supérieure (ENS), Campus Pierre et Marie Curie BC99, 4 place Jussieu, 75005 Paris, France. [21]Institut Universitaire de France, 1 rue Descartes, 75005 Paris, France. [22]Royal Belgian Institute for Space Aeronomy, avenue Circulaire 3, 1180 Brussels, Belgium. [23]Graduate School of Science, Osaka University, Machikaneyama-cho, Toyonaka, Japan. [24]Rikkyo University, 3-34-1 Nishi-Ikebukuro, Toshima, Tokyo 171-8501, Japan. [25]Department of Physics, College of Sciences, University of Central Florida, 4111 Libra Drive, Physical Sciences Bldg. 430, Orlando, FL, USA.

References

Agee CB, Wilson NV, McCubbin FN et al (2013) Unique meteorite from early Amazonian Mars: water-rich basaltic breccia Northwest Africa 7034. Science 339:780–785. https://doi.org/10.1126/science.1228858

Amerstorfer UV, Gröller H, Lichtenegger H, Lammer H, Tian F, Noack L, Scherf M, Johnstone C, Tu L, Guedel M (2017) Escape and evolution of Mars's CO_2 atmosphere: influence of suprathermal atoms. J Geophys Res Planets 122:1321–1337. https://doi.org/10.1002/2016JE005175

Aoki S, Vandaele AC, Daerden F, Villanueva GL, Liuzzi G, Thomas IR, Erwin JT, Trompet L, Robert S, Neary L, Viscardy S, Clancy RT, Smith MD, Lopez-Valverde MA, Hill B, Ristic B, Patel MR, Bellucci G, Lopez-Moreno J-J (2019) Water vapor vertical profiles on Mars in dust storms observed by TGO/NOMAD. J Geophys Res Planets 124(12):3482–3497. https://doi.org/10.1029/2019JE006109

Asamura K, Kazama Y, Yokota S, Kasahara S, Miyoshi Y (2018) Low-energy parti-cle experiments—ion analyzer (LEPi) onboard the ERG (Arase) satellite. Earth Planets Space 70:70. https://doi.org/10.1186/s40623-018-0846-0

Atreya SK, Trainer MG, Franz HB et al (2013) Primordial argon isotope fractiona-tion in the atmosphere of Mars measured by the SAM instrument on curiosity and implications for atmospheric loss. Geophys Res Lett 40:5605–5609. https://doi.org/10.1002/2013GL057763

Avice G, Marty B (2020) Perspectives on atmospheric evolution from noble gas and nitrogen isotopes on earth. Mars Venus Space Sci Rev 216:36

Barabash S, Norberg O (1994) Indirect detection of the Martian helium corona. Geophys Res Lett 21:1547–1550

Barabash S et al (2006) The analyzer of space plasmas and energetic atoms (ASPERA-3) for the Mars Express mission. Space Sci Rev 126:113–164. https://doi.org/10.1007/s11214-006-9124-8

Barucci MA et al (2021) MIRS an Imaging spectrometer for the MMX mission. Earth Planets Space https://doi.org/10.1186/s40623-021-01423-2

Batalha N, Domagal-Goldman SD, Ramirez R, Kasting JF (2015) Testing the early Mars H_2-CO_2 greenhouse hypothesis with a 1-D photochemical model. Icarus 258:337–349. https://doi.org/10.1016/j.icarus.2015.06.016

Batalha NE, Kopparapu RK, Haqq-Misra J, Kasting JF (2016) Climate cycling on early Mars caused by the carbonate–silicate cycle. Earth Planet Sci Lett 455:7–13. https://doi.org/10.1016/j.epsl.2016.08.044

Beaty DW, Grady MM, McSween HY et al (2019) The potential science and engineering value of samples delivered to Earth by Mars sample return: International MSR Objectives and Samples Team (iMOST). Meteorit Planet Sci 54:S3-152. https://doi.org/10.1111/maps.13242

Bell JF, Wolff MJ, Malin MC et al (2009) Mars Reconnaissance Orbiter Mars Color Imager (MARCI): instrument description, calibration, and performance. J Geophys Res 114:1–41. https://doi.org/10.1029/2008JE003315

Bellucci JJ, Nemchin AA, Whitehouse MJ, Humayun R, Zanda B (2015) Pb-isotopic evidence for an early, enriched crust on Mars. Earth Planet Sci Lett 410:34–41. https://doi.org/10.1016/j.epsl.2014.11.018

Bertrand T, Wilson RJ, Kahre MA et al (2020) Simulation of the 2018 global dust storm on mars using the NASA Ames Mars GCM: a multitracer approach. J Geophys Res Planets 125:1–36. https://doi.org/10.1029/2019JE006122

Bibring JP, Soufflot A, Berthé M, Langevin Y, Gondet B, Drossart P, Bouyé M, Combes M, Puget P, Semery A, Bellucci G, Formisano V, Moroz V, Kottsov V, The OMEGA Co-I Team, Bonello G, Erard S, Forni O, Gendrin A, Manaud N, Poulet F, Poulleau G, Encrenaz T, Fouchet T, Melchiori R,

Altieri F, Ignatiev N, Titov D, Zasova L, Coradini A, Capacionni F, Cerroni P, Fonti S, Mangold N, Pinet P, Schmitt B, Sotin C, Hauber E, Hoffmann H, Jaumann R, Keller U, Arvidson R, Mustard J, Forget F (2004) OMEGA: Observatoire pour la Minéralogie, l'Eau, les Glaces et l'Activité in: Wilson A (ed) Mars Express: A European Mission to the Red Planet (ESA SP-1240), ISBN 92-9092-556-6, ISSN 0379-6566, ESA Publications Division Scientific.

Bibring JP, Langevin Y, Mustard JF et al (2006) Global mineralogical and aque-ous mars history derived from OMEGA/Mars express data. Science 312:400–404. https://doi.org/10.1126/science.1122659

Boctor NZ, Alexander CO, Wang J, Hauri E (2003) The sources of water in Mar-tian meteorites: clues from hydrogen isotope. Geochim Cosmochim Acta 67(3971):3989. https://doi.org/10.1016/S0016-7037(03)00234-5

Bogard DD, Johnson P (1983) Martian gases in an Antarctic meteorite? Science 221:651–654. https://doi.org/10.1126/science.221.4611.651

Borg LE, Connelly JN, Nyquist LE, Shih C-Y, Wiesmann H, Reese Y (1999) The age of the carbonates in Martian meteorite ALH84001. Science 286:90–94. https://doi.org/10.1126/science.286.5437.90

Brain D et al (2010) A comparison of global models for the solar wind interac-tion with Mars. Icarus 206:139–151. https://doi.org/10.1016/j.icarus.2009.06.030

Brain DA, McFadden JP, Halekas JS et al (2015) The spatial distribution of planetary ion fluxes near Mars observed by MAVEN. Geophys Res Lett. https://doi.org/10.1002/2015GL065293

Bridges JC, Hicks LJ, Treiman AH (2019) Carbonates on Mars. In: Filiberto J, Schwenzer SP (ed) Volatiles in the Martian crust, Elsevier, pp 89–118. https://doi.org/10.1016/B978-0-12-804191-8.00005-2

Burr DM, Williams RME, Wendell KD et al (2010) Inverted fluvial features in the Aeolis/Zephyria Plana region, Mars: formation mechanism and initial paleodischarge estimates. J Geophys Res Planets. https://doi.org/10.1029/2009JE003496

Carlsson E, Fedorov A, Barabash S et al (2006) Mass composition of the escap-ing plasma at Mars. Icarus 182:320–328. https://doi.org/10.1016/j.icarus.2005.09.020

Carr MH, Head JW III (2010) Geologic history of Mars. Earth Planet Sci Lett 294:185–203. https://doi.org/10.1016/j.epsl.2009.06.042

Carr RH, Grady MM, Wright IP, Pillinger CT (1985) Martian atmospheric carbon dioxide and weathering products in SNC meteorites. Nature 314:248–250. https://doi.org/10.1038/314248a0

Cassata WS (2017) Meteorite constraints on Martian atmospheric loss and paleoclimate. Earth Planet Sci Lett 479:322–329

Cassata WS, Cohen BE, Mark DF et al (2018) Chronology of martian breccia NWA 7034 and the formation of the Martian crustal dichotomy. Sci Adv 4(5):eaap8306. https://doi.org/10.1126/sciadv.aap8306

Clayton RN, Mayeda TK (1996) Oxygen isotope studies of achondrites. Geo-chim Cosmochim Acta 60:1999–2017. https://doi.org/10.1016/0016-7037(96)00074-9

Chaffin M, Deighan J, Schneider N et al (2017) Elevated atmospheric escape of atomic hydrogen from Mars induced by high-altitude water. Nat Geosci 10:174–178. https://doi.org/10.1038/ngeo2887

Chanteur GM, Dubinin E, Modolo R, Fraenz M (2009) Capture of solar wind alpha-particles by the Martian atmosphere. Geophys Res Lett 36:L23105. https://doi.org/10.1029/2009GL040235

Chassefière E, Leblanc F (2004) Mars atmospheric escape and evolution; inter-action with the solar wind. Planet Space Sci 52(11):1039–1058. https://doi.org/10.1016/j.pss.2004.07.002

Chicarro A, Martin P, and Trautner R (2004) The Mars Express mission: an overview. In: Wilson A (ed) Mars Express: A European Mission to the Red Planet (ESA SP-1240), ISBN 92-9092-556-6 ISSN 0379-6566, ESA Publica-tions Division Scientific.

Clarke JT, Bertaux J-L, Chaufray J-Y, Gladstone GR, Quemerais E, Wilson JK, Bhattacharyya D (2014) A rapid decrease of the hydrogen corona of Mars. Geophys Res Lett 41:8013–8020. https://doi.org/10.1002/2014GL061803

Conrad PG, Malespin CA, Franz HB et al (2016) In situ measurement of atmos-pheric krypton and xenon on Mars with Mars Science Laboratory. Earth Planet Sci Lett 454:1–9. https://doi.org/10.1016/j.epsl.2016.08.028

Craddock RA, Howard AD (2002) The case for rainfall on a warm, wet early Mars. J Geophys Res Planets. https://doi.org/10.1029/2001JE001505

Cui J, Wu X-S, Gu H, Jiang F-Y, Wei Y (2019) Photochemical escape of atomic C and N on Mars: clues from a multi-instrument MAVEN dataset. Astron Astrophys 621:A23. https://doi.org/10.1051/0004-6361/201833749

Davis JM, Balme M, Grindrod PM et al (2016) Extensive Noachian fluvial sys-tems in Arabia Terra: implications for early Martian climate. Geology 44:847–850. https://doi.org/10.1130/G38247.1

Davis JM, Gupta S, Balme M, Grindrod PM, Fawdon P, Dickeson ZI, Williams RM (2019) A diverse array of fluvial depositional systems in Arabia Terra: evidence for mid-Noachian to early Hesperian rivers on Mars. J Geophys Res Planets 124(7):1913–1934

Delcourt D et al (2016) The Mass Composition Analyzer (MSA) on board the BepiColombo MMO. J Geophys Res Space Phys 121(7):6749–6762

DiBraccio GA, Dann J, Espley JR et al (2017) MAVEN observations of tail current sheet flapping at Mars. J Geophys Res Space Phys 122:4308–4324. https://doi.org/10.1002/2016JA023488

Dong Y, Fang X, Brain DA, McFadden JP, Halekas JS, Connerney JE, Curry SM, Harada Y, Luhmann JG, Jakosky BM (2015) Strong plume fluxes at Mars observed by MAVEN: an important planetary ion escape chan-nel. Geophys Res Lett. https://doi.org/10.1002/2015GL065346

Dong Y, Fang X, Brain DA, McFadden JP, Halekas JS, Connerney JEP, Eparvier F, Andersson L, Mitchell D, Jakosky BM (2017) Seasonal variability of Martian ion escape through the plume and tail from MAVEN observa-tions. J Geophys Res Space Phys. https://doi.org/10.1002/2016JA023517

Dong C, Bougher SW, Ma Y, Lee Y, Toth G, Nagy AF et al (2018) Solar wind interaction with the Martian upper atmosphere: roles of the cold thermosphere and hot oxygen corona. J Geophys Res Space Phys 123:6639–6654. https://doi.org/10.1029/2018JA025543

Dubinin E, Fraenz M, Woch J, Duru F, Gurnett D, Modolo R, Barabash S, Lun-din R (2009) Ionospheric storms on Mars: impact of the corotating interaction region. Geophys Res Lett 36:L01105. https://doi.org/10.1029/2008GL036559

Dubinin E et al (2011) Ion energization and escape on Mars and Venus. In: Szego K (ed) The plasma environment of Venus, Mars, and Titan. Space Sciences Series of ISSI, vol 37. Springer, New York, https://doi.org/10.1007/978-1-4614-3290-6_6

Dundas CM, Bramson AM, Ojha L et al (2018) Exposed subsurface ice sheets in the Martian mid-latitudes. Science 359:199–201. https://doi.org/10.1126/science.aao1619

Edberg NJT, Nilsson H, Williams AO, Lester M, Milan SE, Cowley SWH, Fränz M, Barabash S, Futaana Y (2010) Pumping out the atmosphere of Mars through solar wind pressure pulses. Geophys Res Lett 37:L03107. https://doi.org/10.1029/2009GL041814

Ehlmann BL, Edwards CS (2014) Mineralogy of the Martian surface. Ann Rev Earth Planet Sci 42:291–315. https://doi.org/10.1146/annurev-earth-060313-055024

Ehlmann BL, Mustard JF, Murchie SL, Bibring JP, Meunier A, Fraeman AA, Langevin Y (2011) Subsurface water and clay mineral formation dur-ing the early history of Mars. Nature 479:53–60. https://doi.org/10.1038/nature10582

Fang X, Liemohn MW, Nagy AF, Ma Y, De Zeeuw DL, Kozyra JU, Zurbuchen TH (2008) Pickup oxygen ion velocity space and spatial distribution around Mars. J Geophys Res 113:A02210. https://doi.org/10.1029/2007JA012736

Fang X et al (2017) The mars crustal magnetic field control of plasma boundary locations and atmospheric loss: MHD prediction and comparison with MAVEN. J Geophys Res Space Phys. https://doi.org/10.1002/2016JA023509

Fassett CI, Head JW (2008a) Valley network-fed, open-basin lakes on Mars: distribution and implications for Noachian surface and subsurface hydrology. Icarus 198:37–56. https://doi.org/10.1016/j.icarus.2008.06.016

Fassett CI, Head JW III (2008b) The timing of Martian valley network activity: constraints from buffered crater counting. Icarus 195(1):61–89. https://doi.org/10.1016/j.icarus.2007.12.009

Fedorova A, Bertaux JL, Betsis D et al (2018) Water vapor in the middle atmos-phere of Mars during the 2007 global dust storm. Icarus 300:440–457. https://doi.org/10.1016/j.icarus.2017.09.025

Fedorova A, Montmessin F, Korablev O, Luginin M, Trokhimovskiy A, Belyaev D, Ignatiev N, Lefèvre F, Alday J, Irwin P, Olsen K, Bertaux J-L, Millour E, Maattanen A, Shakun A, Grigoriev A, Patrakeev A, Korsa S, Kokonkov N,

Ogohara *et al. Earth, Planets and Space*   (2022) 74:1

Page 27 of 32

Baggio L, Forget F, Wilson C (2020) Stormy water on Mars: the distribution and saturation of atmospheric water during the dusty season. Science 367(6475):297–300. https://doi.org/10.1126/science.aay9522

Fenton LK, Geissler PE, Haberle RM (2007) Global warming and climate forcing by recent albedo changes on Mars. Nature 446:646–649. https://doi.org/10.1038/nature05718

Forget F, Pierrehumbert RT (1997) Warming early mars with carbon dioxide clouds that scatter infrared radiation. Science 278:1273–1276. https://doi.org/10.1126/science.278.5341.1273

Forget F, Wordsworth R, Millour E et al (2013) 3D modelling of the early Martian climate under a denser CO_2 atmosphere: temperatures and CO_2 ice clouds. Icarus 222:81–99. https://doi.org/10.1016/j.icarus.2012.10.019

Fouchet T, Lellouch E, Ignatiev NI et al (2007) Martian water vapor: Mars Express PFS/LW observations. Icarus 190:32–49. https://doi.org/10.1016/j.icarus.2007.03.003

Futaana Y et al (2008) Mars Express and Venus Express multi-point observations of geoeffective solar flare events in December 2006. Planet Space Sci 56:873–880

Giuranna M, Wolkenberg P, Grassi D et al (2021) The current weather and climate of Mars: 12 years of atmospheric monitoring by the Planetary Fourier Spectrometer on Mars Express. Icarus 353:113406. https://doi.org/10.1016/j.icarus.2019.113406

Godin PJ, Ramirez RM, Campbell CL et al (2020) Collision-induced absorption of CH_4-CO_2 and H_2-CO_2 complexes and their effect on the ancient Martian atmosphere. J Geophys Res Planets 125:1–10. https://doi.org/10.1029/2019JE006357

Greenwood JP, Itoh S, Sakamoto N, Vicenzi E, Yurimoto H (2008) Hydrogen isotope evidence for loss of water from Mars through time. Geophys Res Lett 35:L05203. https://doi.org/10.1029/2007GL032721

Gröller H, Lichtenegger H, Lammer H, Shematovich VI (2014) Hot oxygen and carbon escape from the martian atmosphere. Planet Space Sci 98:93–105. https://doi.org/10.1016/j.pss.2014.01.007

Grotzinger JP, Gupta S, Malin MC, Rubin DM, Schieber J, Siebach K, Sumner DY, Stack KM, Vasavada AR, Arvidson RE, Calef F (2015) Deposition, exhumation, and paleoclimate of an ancient lake deposit, Gale crater. Science. https://doi.org/10.1126/science.aac7575

Gu H, Cui J, Niu D, He Z, Li K (2020) Monte Carlo calculations of helium escape on Mars via Energy transfer from hot oxygen atoms. ApJ 902:121

Guzewich SD, Toigo AD, Wang H (2017) An investigation of dust storms observed with the Mars Color Imager. Icarus 289:199–213. https://doi.org/10.1016/j.icarus.2017.02.020

Haberle RM, Kahre MA, Hollingsworth JL et al (2019a) Documentation of the NASA/Ames legacy mars global climate model: simulations of the present seasonal water cycle. Icarus 333:130–164. https://doi.org/10.1016/j.icarus.2019.03.026

Haberle RM, Zahnle K, Barlow NG, Steakley KE (2019b) Impact degassing of H_2 on early Mars and its effect on the climate system. Geophys Res Lett 46:13355–13362. https://doi.org/10.1029/2019GL084733

Halevy I, Head JW (2014) Episodic warming of early Mars by punctuated volcanism. Nat Geosci 7:865–868. https://doi.org/10.1038/ngeo2293

Halevy I, Fischer WW, Eiler JM (2011) Carbonates in the Martian meteorite Allan Hills 84001 formed at 18 ± 4 °C in a near-surface aqueous environment. PNAS 108:16895–16899. https://doi.org/10.1073/pnas.1109444108

Hara T, Seki K, Futaana Y, Yamauchi M, Yagi M, Matsumoto Y, Tokumaru M, Fedorov A, Barabash S (2011) Heavy-ion flux enhancement in the vicinity of the Martian ionosphere during CIR passage: Mars Express ASPERA-3 observations. J Geophys Res 116:A02309. https://doi.org/10.1029/2010JA015778

Hara T et al (2015) Estimation of the spatial structure of a detached magnetic flux rope at Mars based on simultaneous MAVEN plasma and magnetic field measurements. Geophys Res Lett. https://doi.org/10.1002/2015GL065720

Hara T et al (2016) MAVEN observations of a giant ionospheric flux rope near Mars resulting from interaction between the crustal and interplanetary draped magnetic fields. J Geophys Res Space Phys. https://doi.org/10.1002/2016JA023347

Harada Y et al (2015) Magnetic reconnection in the near-Mars magnetotail: MAVEN observations. Geophys Res Lett. https://doi.org/10.1002/2015GL065004

Harada Y et al (2017) Survey of magnetic reconnection signatures in the Martian magnetotail with MAVEN. J Geophys Res Space Phys 122:5114–5131. https://doi.org/10.1002/2017JA023952

Harada Y, Halekas JS, DiBraccio GA, Xu S, Espley J, McFadden JP et al (2018) Magnetic reconnection on dayside crustal magnetic fields at Mars: MAVEN observations. Geophys Res Lett 45:4550–4558. https://doi.org/10.1002/2018GL077281

Harada Y, Halekas JS, Xu S, DiBraccio GA, Ruhunusiri S, Hara T et al (2020) Ion jets within current sheets in the Martian magnetosphere. J Geophys Res Space Phys 125:e2020JA028576. https://doi.org/10.1029/2020JA028576

Harnett EM, Winglee RM (2006) Three-dimensional multifluid simulations of ionospheric loss at Mars from nominal solar wind conditions to magnetic cloud events. J Geophys Res 111:A09213. https://doi.org/10.1029/2006JA011724

Hayworth BPC, Kopparapu RK, Haqq-Misra J et al (2020) Warming early Mars with climate cycling: the effect of CO_2-H_2 collision-induced absorption. Icarus 345:113770. https://doi.org/10.1016/j.icarus.2020.113770

Heavens NG, Kleinböhl A, Chaffin MS, Halekas JS, Kass DM, Hayne PO, McCleese DJ, Piqueux S, Shirley JH, Schofield JT (2018) Hydrogen escape from Mars enhanced by deep convection in dust storms. Nat Astron 2:126–132. https://doi.org/10.1038/s41550-017-0353-4

Heavens NG, Kass DM, Shirley JH et al (2019) An observational overview of dusty deep convection in Martian dust storms. J Atmos Sci 76:3299–3326. https://doi.org/10.1175/JAS-D-19-0042.1

Hennen M, White K, Shahgedanova M (2019) An assessment of SEVIRI imagery at various temporal resolutions and the effect on accurate dust emission mapping. Remote Sens 11(8):918. https://doi.org/10.3390/rs11080965

Hinson DP, Tyler D, Lewis SR et al (2019) The Martian daytime convective boundary layer: results from radio occultation measurements and a mesoscale model. Icarus 326:105–122. https://doi.org/10.1016/j.icarus.2019.02.028

Hoke MR, Hynek BM, Tucker GE (2011) Formation timescales of large Martian valley networks. Earth Planet Sci Lett 312:1–12

Howard AD, Moore JM, Irwin RP (2005) An intense terminal epoch of widespread fluvial activity on early Mars: 1. Valley network incision and associated deposits. J Geophys Res Planets 110:1–20. https://doi.org/10.1029/2005JE002459

Hu S, Lin Y, Zhang J et al (2014) NanoSIMS analyses of apatite and melt inclusions in the GRV 020090 Martian meteorite: Hydrogen isotope evidence for recent past underground hydrothermal activity on Mars. Geochim Cosmochim Acta 140:321–333. https://doi.org/10.1016/j.gca.2014.05.008

Hu R, Kass DM, Ehlmann BL, Yung YL (2015) Tracing the fate of carbon and the atmospheric evolution of Mars. Nat Commun 6:10003. https://doi.org/10.1038/ncomms10003

Humayun M, Nemchin A, Zanda B et al (2013) Origin and age of the earliest Martian crust from meteorite NWA 7533. Nature 503:513–516. https://doi.org/10.1038/nature12764

Hyodo R, Genda H, Charnoz S, Rosenblatt P (2017) On the impact origin of Phobos and Deimos. I. Thermodynamic and physical aspects. Astrophys J 845:125. https://doi.org/10.3847/1538-4357/aa81c4

Hyodo R, Kurosawa K, Genda H, Usui T, Fujita K (2019) transport of impact ejecta from Mars to its moons as a means to reveal Martian history. Sci Rep 9:19833. https://doi.org/10.1038/s41598-019-56139-x

Inada A, Garcia-Comas M, Altieri F et al (2008) Dust haze in Valles Marineris observed by HRSC and OMEGA on board Mars Express. J Geophys Res 113:1–18. https://doi.org/10.1029/2007JE002893

Inui S, Seki K, Namekawa T et al (2018) Cold dense ion outflow observed in the Martian-induced magnetotail by MAVEN. Geophys Res Lett 45:5283–5289. https://doi.org/10.1029/2018GL077584

Inui S, Seki K, Sakai S et al (2019) Statistical study of heavy ion outflows from Mars observed in the Martian-induced magnetotail by MAVEN. J Geophys Res Space Phys 124:5482–5497. https://doi.org/10.1029/2018JA026452

Irwin RP, Craddock RA, Howard AD, Flemming HL (2011) Topographic influences on development of Martian valley networks. J Geophys Res Planets. https://doi.org/10.1029/2010JE003620

Ogohara *et al. Earth, Planets and Space* (2022) 74:1

Page 28 of 32

Ito Y, Hashimoto GL, Takahashi YO, Ishiwatari M, Kuramoto K (2020) H_2O_2-induced greenhouse warming on oxidized early Mars. Astrophys J 893(2):168

Jakosky BM, Jones JH (1997) The history of Martian volatiles. Rev Geophys 35:1–16. https://doi.org/10.1029/96RG02903

Jakosky BM, Lin RP, Grebowsky JM et al (2015) The mars atmosphere and volatile evolution (MAVEN) mission. Space Sci Rev 195:3–48. https://doi.org/10.1007/s11214-015-0139-x

Jakosky BM, Slipski M, Benna M et al (2017) Mars' atmospheric history derived from upper-atmosphere measurements of 38Ar/36Ar. Science 355:1408–1410. https://doi.org/10.1126/science.aai7721

Jakosky BM, Brain D, Chaffin M et al (2018) Loss of the Martian atmosphere to space: present-day loss rates determined from MAVEN observations and integrated loss through time. Icarus 315:146–157. https://doi.org/10.1016/j.icarus.2018.05.030

Kamada A, Kuroda T, Kasaba Y et al (2020) A coupled atmosphere–hydrosphere global climate model of early Mars: a 'cool and wet' scenario for the formation of water channels. Icarus 338:113567. https://doi.org/10.1016/j.icarus.2019.113567

Kameda S, Suzuki H, Takamatsu T et al (2017) Preflight calibration test results for optical navigation camera telescope (ONC-T) onboard the Hayabusa2 spacecraft. Space Sci Rev 208:17–31

Kameda S et al (2021) Design of telescopic nadir imager for geomorphology (TENGOO) and observation of surface reflectance by optical chromatic imager (OROCHI) for the Martian Moons Exploration (MMX). Earth Planets Space. https://doi.org/10.1186/s40623-021-01462-9

Kasting JF (1991) CO_2 condensation and the climate of early Mars. Icarus 94(1):1–13

Kawakatsu Y (2018) Mission design of Martian Moons eXploration (MMX). In: Paper presented at the 69th international astronautical congress. IAC-18-A3.3A.8.x47632, Bremen, 1–5 October 2018

Kawakatsu Y, Kuramoto K, Ogawa N, Ikeda H, Mimasu Y, Ono G, Sawada H, Yoshikawa K, Imada T, Otake H, Kusano H, Yamada K, Otsuki M, Baba M (2017) Mission concept of Martian moons exploration (MMX). In: Proceedings in the 68th international astronautical congress, IAC-17-A3-3A.5.x40742. Adelaide, 25–29 September 2017

Kerber L, Forget F, Wordsworth R (2015) Sulfur in the early Martian atmosphere revisited: experiments with a 3-D Global Climate Model. Icarus 261:133–148. https://doi.org/10.1016/j.icarus.2015.08.011

Kite ES, Halevy I, Kahre MA et al (2013) Seasonal melting and the formation of sedimentary rocks on Mars, with predictions for the Gale Crater mound. Icarus 223:181–210. https://doi.org/10.1016/j.icarus.2012.11.034

Kite ES, Mischna MA, Gao P et al (2020) Methane release on Early Mars by atmospheric collapse and atmospheric reinflation. Planet Space Sci 181:104820. https://doi.org/10.1016/j.pss.2019.104820

Kitzmann D (2016) Revisiting the scattering greenhouse effect of CO_2 ice clouds. Astrophys J 817:L18. https://doi.org/10.3847/2041-8205/817/2/l18

Kleinböhl A, Schofield JT, Kass DM, Abdou WA, Backus CR, Sen B, Shirley JH, Lawson WG, Richardson MI, Taylor FW, Teanby NA, McCleese DJ (2009) Mars Climate Sounder limb profile retrieval of atmospheric temperature, pressure, and dust and water ice opacity. J Geophys Res 114(E10):E10006

Kleinböhl A, Spiga A, Kass DM et al (2020) Diurnal variations of dust during the 2018 global dust storm observed by the mars climate sounder. J Geophys Res Planets 125:1–21. https://doi.org/10.1029/2019JE006115

Koike M, Nakada R, Kajitani I, Usui T, Tamenori Y, Sugahara H, Kobayashi A (2020) In-situ preservation of nitrogen-bearing organics in Noachian Martian carbonates. Nat Commun 11:1988. https://doi.org/10.1038/s41467-020-15931-4

Korablev O, Montmessin F, Trokhimovskiy A et al (2018) The atmospheric chemistry suite (ACS) of three spectrometers for the ExoMars 2016 trace gas orbiter. Space Sci Rev 214:7. https://doi.org/10.1007/s11214-017-0437-6

Kounaves SP, Oberlin EA (2019) Volatiles measured by the phoenix lander at the northern plains of Mars. In: Filiberto J, Schwenzer SP (eds) Volatiles in the Martian crust, Elsevier, pp 265–283. https://doi.org/10.1016/B978-0-12-804191-8.00009-X

Kounaves SP, Carrier BL, O'Neil GD et al (2014) Evidence of martian perchlorate, chlorate, and nitrate in Mars meteorite EETA79001: implications for

oxidants and organics. Icarus 229:206–213. https://doi.org/10.1016/j.icarus.2013.11.012

Krasnopolsky VA, Gladstone GR (1996) Helium on Mars: EUVE and PHOBOS data and implications for Mars' evolution. J Geophys Res 101:15765–15772

Kulowski L, Wang H, Toigo AD (2017) The seasonal and spatial distribution of textured dust storms observed by Mars Global Surveyor Mars Orbiter Camera. Adv Space Res 59:715–721. https://doi.org/10.1016/j.asr.2016.10.028

Kuramoto K et al (2021) Martian moons exploration MMX: sample return mission to Phobos elucidating formation processes of habitable planets. Earth Planets Space. https://doi.org/10.1186/s40623-021-01545-7

Kurokawa H, Sato M, Ushioda M, Matsuyama T, Moriwaki R, Dohm JM, Usui T (2014) Evolution of water reservoirs on Mars: constraints from hydrogen isotopes in martian meteorites. Earth Planet Sci Lett 394:179–185. https://doi.org/10.1016/j.epsl.2014.03.027

Kurokawa H, Kurosawa K, Usui T (2018) A lower limit of atmospheric pressure on early Mars inferred from nitrogen and argon isotopic compositions. Icarus 299:443–459. https://doi.org/10.1016/j.icarus.2017.08.020

Lammer H, Chassefière E, Karatekin Ö et al (2013) Outgassing history and escape of the Martian atmosphere and water inventory. Space Sci Rev 174:113–154. https://doi.org/10.1007/s11214-012-9943-8

Lammer H, Scherf M, Kurokawa H et al (2020) Loss and fractionation of noble gas isotopes and moderately volatile elements from planetary embryos and early venus. Earth Mars Space Sci Rev 216:74. https://doi.org/10.1007/s11214-020-00701-x

Lapen TJ, Righter M, Brandon AD, Debaille V, Beard BL, Shafer JT, Peslier AH (2010) A younger age for ALH84001 and its geochemical link to shergottite sources in Mars. Science 328:347–351. https://doi.org/10.1126/science.1185395

Lee Y, Fang X, Gacesa M et al (2020) Effects of global and regional dust storms on the Martian hot O corona and photochemical loss. J Geophys Res Space Phys 125:e2019JA027115. https://doi.org/10.1029/2019JA027115

Leshin LA (2000) Insights into Martian water reservoirs from analyses of Martian meteorite QUE94201. Geophys Res Lett 27:2017–2020. https://doi.org/10.1029/1999GL008455

Leshin LA, Mahaffy PR, Webster CR et al (2013) Volatile, isotope, and organic analysis of Martian fines with the Mars curiosity rover. Science 341:1238937. https://doi.org/10.1126/science.1238937

Liuzzi G, Villanueva G, Crismani M, Smith MD, Mumma M, Daerden F, Aoki S, Vandaele AC, Clancy R, Erwin J, Thomas IR, Ristic B, Lopez-Moreno J-J, Bellucci G, Patel M (2020) Strong variability of Martian water ice clouds during dust storms revealed from ExoMars trace gas orbiter/NOMAD. J. Geophys. Res. Planets 125(4):e2019JE006250. https://doi.org/10.1029/2019JE006250

Lundin R (2011) Ion acceleration and outflow from mars and venus: an overview. In: Szego K (ed) The plasma environment of Venus, Mars, and Titan. Space Sciences Series of ISSI, vol 37. Springer, New York. https://doi.org/10.1007/978-1-4614-3290-6_9

Lundin R, Dubinin EM (1992) Phobos-2 results on the ionospheric plasma escape from Mars. Adv Space Res 12(9):255–263

Lundin R, Zakharov A, Pellinen R et al (1989) First measurements of the ionospheric plasma escape from Mars. Nature 341:609–612. https://doi.org/10.1038/341609a0

Lundin R et al (1990) ASPERA/PHOBOS measurements of the ion outflow from the Martian ionosphere. Geophys Res Lett 17(6):873–876

Lundin R, Barabash S, Fedorov A, Holmström M, Nilsson H, Sauvaud JA, Yamauchi M (2008) Solar forcing and planetary ion escape from Mars. Geophys Res Lett 35:L09203. https://doi.org/10.1029/2007GL032884

Lundin R, Barabash S, Holmström M, Nilsson H, Yamauchi M, Dubinin EM, Fraenz M (2009) Atmospheric origin of cold ion escape from Mars. Geophys Res Lett 36:L17202. https://doi.org/10.1029/2009GL039341

Ma Y, Nagy AF, Sokolov IV, Hansen KC (2004) Three-dimensional, multispecies, high spatial resolution MHD studies of the solar wind interaction with Mars. J Geophys Res 109:A07211. https://doi.org/10.1029/2003JA010367

Ma YJ et al (2015) MHD model results of solar wind interaction with mars and comparison with MAVEN plasma observations. Geophys Res Lett 42:9113–9120. https://doi.org/10.1002/2015GL065218

Ma YJ et al (2017) Variations of the Martian plasma environment during the ICME passage on 8 March 2015: a time-dependent MHD study. J

Ogohara *et al. Earth, Planets and Space*   (2022) 74:1

Page 29 of 32

Geophys Res Space Phys 122:1714–1730. https://doi.org/10.1002/2016JA023402

Mahaffy PR, Webster CR, Stern JC et al (2015) The imprint of atmospheric evolution in the D/H of Hesperian clay minerals on Mars. Science 347:412–414. https://doi.org/10.1126/science.1260291

Malin MC, Bell JF III, Cantor BA, Caplinger MA, Calvin WM, Clancy RT, Edgett KS, Edwards L, Haberle RM, James PB, Lee SW, Ravine MA, Thomas PC, Wolff MJ (2007) Context camera investigation on board the Mars reconnaissance orbiter. J Geophys Res 112:E05S04. https://doi.org/10.1029/2006JE002808

Malin MC, Harrison TN, Edgett KS (2009) Martian weather activity on short timescales, Malin space science systems captioned image release, MSSS-70, http://www.msss.com/msss_images/2009/02/23/

Maltagliati L, Titov DV, Encrenaz T et al (2008) Observations of atmospheric water vapor above the Tharsis volcanoes on Mars with the OMEGA/MEx imaging spectrometer. Icarus 194:53–64. https://doi.org/10.1016/j.icarus.2007.09.027

Maltagliati L, Titov DV, Encrenaz T et al (2011) Annual survey of water vapor behavior from the OMEGA mapping spectrometer onboard Mars Express. Icarus 213:480–495. https://doi.org/10.1016/j.icarus.2011.03.030

Masunaga K, Seki K, Brain DA, Fang X, Dong Y, Jakosky BM, McFadden JP, Halekas JS, Connerney JEP (2016) O+ ion beams reflected below the Martian bow shock: MAVEN observations. J Geophys Res Space Phys 121:3093–3107. https://doi.org/10.1002/2016JA022465

Masunaga K et al (2017) Statistical analysis of the reflection of incident O+ pickup ions at Mars: MAVEN observations. J Geophys Res Space Phys 122:4089–4101. https://doi.org/10.1002/2016JA023516

Masunaga K, Yoshioka K, Chaffin MS, Deighan J, Jain SK, Schneider NM et al (2020) Martian oxygen and hydrogen upper atmospheres responding to solar and dust storm drivers: Hisaki space telescope observations. J Geophys Res Planets 125:e2020JE006500. https://doi.org/10.1029/2020JE006500

Masursky H (1973) An overview of geological results from Mariner 9. J Geophys Res 78(20):4009–4030

Mathew KJ, Marti K (2001) Early evolution of Martian volatiles'nitrogen and noble gas components in ALH84001 and Chassigny. J Geophys Res 106:1401–1422

Matsuoka A et al (2018) The ARASE (ERG) magnetic field investigation. Earth Planets Space 70:43. https://doi.org/10.1186/s40623-018-0800-1

McCubbin FM, Boyce JW, Srinivasan P et al (2016) Heterogeneous distribution of H_2O in the Martian interior: implications for the abundance of H_2O in depleted and enriched mantle sources. Meteoritics Planet Sci 51:2036–2060. https://doi.org/10.1111/maps.12639

McFadden JP et al (2015) MAVEN SupraThermal and thermal ion composition (STATIC) instrument. Space Sci Rev. https://doi.org/10.1007/s11214-015-0175-6

McSween HY Jr (2015) Petrology on Mars. Am Miner 100:2380–2395. https://doi.org/10.2138/am-2015-5257

McSween Jr HY, McLennan SM (2014) 2.10 Mars. In: Holland HD, Turekian KK (eds) Treatise on geochemistry, 2nd ed, Elsevier Science, pp 251–300. https://doi.org/10.1016/B978-0-08-095975-7.00125-X

Melchiorri R, Encrenaz T, Drossart P et al (2009) OMEGA/Mars Express: South Pole Region, water vapor daily variability. Icarus 201:102–112. https://doi.org/10.1016/j.icarus.2008.12.018

Mischna MA, Baker V, Milliken R et al (2013) Effects of obliquity and water vapor/trace gas greenhouses in the early Martian climate. J Geophys Res Planets 118:560–576. https://doi.org/10.1002/jgre.20054

Mitrofanov I, Malakhov A, Bakhtin B, Golovin D, Kozyrev A, Litvak M, Mokrousov M, Sanin A, Tretyakov V, Vostrukhin A, Anikin A, Zelenyi LM, Semkova J, Malchev S, Tomov B, Matviichuk Y, Dimitrov P, Koleva R, Dachev T, Krastev K, Shvetsov V, Timoshenko G, Bobrovnitsky Y, Tomilina T, Benghin V, Shurshakov V (2018) Fine resolution epithermal neutron detector (FREND) onboard the ExoMars trace gas orbiter. Space Sci Rev 214:86. https://doi.org/10.1007/s11214-018-0522-5

Mittlefehldt DW (1994) ALH84001, a cumulate orthopyroxenite member of the Martian meteorite clan. Meteoritics 29:214–221. https://doi.org/10.1111/j.1945-5100.1994.tb00673.x

Modolo R et al (2016) Mars-solar wind interaction: LatHyS, an improved parallel 3-D multispecies hybrid model. J Geophys Res Space Phys 121:6378–6399. https://doi.org/10.1002/2015JA022324

Montabone L, Spiga A, Kass DM et al (2020) Martian year 34 column dust climatology from Mars climate sounder observations: reconstructed maps and model simulations. J Geophys Res Planets. https://doi.org/10.1029/2019je006111

Montmessin F, Korablev O, Lefèvre F et al (2017) SPICAM on Mars Express: a 10 year in-depth survey of the Martian atmosphere. Icarus 297:195–216. https://doi.org/10.1016/j.icarus.2017.06.022

Mouginot J, Pommerol A, Beck P, Kofman W, Clifford SM (2012) Dielectric map of the Martian northern hemisphere and the nature of plain filling materials. Geophys Res Lett 39:L02202. https://doi.org/10.1029/2011GL050286

Murchie S, Erard S (1996) Spectral properties and heterogeneity of Phobos from measurements by Phobos 2. Icarus 123:63–86. https://doi.org/10.1006/icar.1996.0142

Nakada R, Usui T, Ushioda M, Takahashi Y (2020) Vanadium micro-XANES determination of oxygen fugacity in olivine-hosted glass inclusion and groundmass glasses of Martian primitive basalt Yamato 980459. Am Miner 105(11):1695–1703. https://doi.org/10.2138/am-2020-7321

Nakagawa H (2019) Atmosphere of Mars. In: Yamagishi A, Kakegawa T, Usui T (eds) Astrobiology. Springer, Heidelberg, p 353

Navarro T, Madeleine J, Forget F et al (2014) Global climate modeling of the Martian water cycle with improved microphysics and radiatively active water ice clouds. J Geophys Res Planets 119:1479–1495. https://doi.org/10.1002/2013JE004550.Received

Nayak M, Nimmo F, Udrea B (2016) Effects of mass transfer between Martian satellites on surface geology. Icarus 267:220–231. https://doi.org/10.1016/j.icarus.2015.12.026

Neary L, Daerden F, Aoki S et al (2020) Explanation for the increase in high-altitude water on Mars observed by NOMAD during the 2018 global dust storm. Geophys Res Lett 47:1–9. https://doi.org/10.1029/2019GL084354

Neukum G, Jaumann R, The HRSC Co-Investigator and Experiment Team (2004) HRSC: the high resolution stereo camera of Mars Express. In: Wilson A (ed) Mars Express: a European Mission to the Red Planet (ESA SP-1240) ISBN 92-9092-556-6, ISSN 0379-6566, ESA Publications Division Scientific

Neumann GA, Rowlands DD, Lemoine FG, Smith DE, Zuber MT (2001) Crossover analysis of Mars orbiter laser altimeter data. J Geophys Res 106(E10):23753–23768. https://doi.org/10.1029/2000JE001381

Neumann GA, Smith DE, Zuber MT (2003) Two Mars years of clouds detected by the Mars Orbiter Laser Altimeter. J Geophys Res 108(E4):5023. https://doi.org/10.1029/2002JE001849

Niles PB, Leshin LA, Guan Y (2005) Microscale carbon isotope variability in ALH84001 carbonates and a discussion of possible formation environments. Geochim Cosmochim Acta 69:2931–2944. https://doi.org/10.1016/j.gca.2004.12.012

Nilsson H et al (2010) Ion escape from mars as a function of solar wind conditions: a statistical study. Icarus 206:40–49

Nilsson H et al (2011) Heavy ion escape from mars, influence from solar wind conditions, and magnetic fields. Icarus 215:475–484

Nilsson H, Stenberg G, Futaana Y et al (2012) Ion distributions in the vicinity of Mars: signatures of heating and acceleration processes. Earth Planets Space 64:135–148. https://doi.org/10.5047/eps.2011.04.011

Nyquist LE, Bogard DD, Shih C-Y, Greshake A, Stöffler D, Eugster O (2001) Ages and geologic histories of Martian meteorites. Space Sci Rev 96:105–164. https://doi.org/10.1023/A:1011993105172

Nyquist LE, Shih C-Y, McCubbin FM et al (2016) Rb-Sr and Sm-Nd isotopic and REE studies of igneous components in the bulk matrix domain of Martian breccia Northwest Africa 7034. Meteorit Planet Sci 51:483–498. https://doi.org/10.1111/maps.12606

Ogohara K, Satomura T (2011) Numerical simulations of the regional characteristics of dust transport on Mars. Adv Space Res 48:1279–1294. https://doi.org/10.1016/j.asr.2011.06.008

Orofino V, Alemanno G, di Achille G, Mancarella F (2018) Estimate of the water flow duration in large Martian fluvial systems. Planet Space Sci 163:83–96. https://doi.org/10.1016/j.pss.2018.06.001

Owen T, Maillard JP, Bergh C, Lutz BL (1988) Deuterium on Mars: the abundance of HDO and the value of D/H. Science 240:1767–1770. https://doi.org/10.1126/science.240.4860.1767

Pepin RO (1991) On the origin and early evolution of terrestrial planet atmospheres and meteoritic volatiles. Icarus 92:2–79

Ogohara *et al. Earth, Planets and Space*   (2022) 74:1

Page 30 of 32

Pollack JB, Kasting JF, Richardson SM, Poliakoff K (1987) The case for a wet, warm climate on early Mars. Icarus 71(2):203–224. https://doi.org/10.1016/0019-1035(87)90147-3

Postawko SE, Kuhn WR (1986) Effect of the greenhouse gases (CO_2, H_2O, SO_2) on Martian paleoclimate. J Geophys Res Solid Earth 91:431–438. https://doi.org/10.1029/jb091ib04p0d431

Pottier A, Forget F, Montmessin F et al (2017) Unraveling the Martian water cycle with high-resolution global climate simulations. Icarus 291:82–106. https://doi.org/10.1016/j.icarus.2017.02.016

Rafkin SCR, Magdalena MRV, Michaels TI (2002) Simulation of the atmospheric thermal circulation of a Martian volcano using a mesoscale numerical model. Nature 419:697–699. https://doi.org/10.1038/nature01114

Rahmati A et al (2017) MAVEN measured oxygen and hydrogen pickup ions: probing the Martian exosphere and neutral escape. J Geophys Res Space Phys. https://doi.org/10.1002/2016JA023371

Rahmati A, Larson DE, Cravens TE, Lillis RJ, Halekas JS, McFadden JP et al (2018) Seasonal variability of neutral escape from Mars as derived from MAVEN pickup ion observations. J Geophys Res Planets. https://doi.org/10.1029/2018JE005560

Ramirez RM (2017) A warmer and wetter solution for early Mars and the challenges with transient warming. Icarus 297:71–82. https://doi.org/10.1016/j.icarus.2017.06.025

Ramirez RM, Craddock RA (2018) The geological and climatological case for a warmer and wetter early Mars. Nat Geosci 11:230–237

Ramirez RM, Kasting JF (2017) Could cirrus clouds have warmed early Mars? Icarus 281:248–261. https://doi.org/10.1016/j.icarus.2016.08.016

Ramirez RM, Kopparapu R, Zugger ME et al (2014) Warming early Mars with CO_2 and H_2. Nat Geosci 7:59–63. https://doi.org/10.1038/ngeo2000

Ramirez RM, Craddock RA, Usui T (2020) Climate simulations of early Mars with estimated precipitation, runoff, and erosion rates. J Geophys Res Planets. https://doi.org/10.1029/2019JE006160

Ramsley KR, Head JW III (2013) Mars impact ejecta in the regolith of Phobos: bulk concentration and distribution. Planet Space Sci 87:115–129. https://doi.org/10.1016/j.pss.2013.09.005

Ramstad R, Barabash S, Futaana Y, Nilsson H, Wang X-D, Holmström M (2015) The Martian atmospheric ion escape rate dependence on solar wind and solar EUV conditions: 1. Seven years of Mars Express observations. J Geophys Res Planets 120:1298–1309. https://doi.org/10.1002/2015JE004816

Ramstad R, Barabash S, Futaana Y, Nilsson H, Holmström M (2017) Global Mars-solar wind coupling and ion escape. J Geophys Res Space Phys 122:8051–8062. https://doi.org/10.1002/2017JA024306

Ramstad R, Barabash S, Futaana Y, Nilsson H, Holmström M (2018) Ion escape from Mars through time: an extrapolation of atmospheric loss based on 10 years of Mars Express measurements. J Geophys Res Planets 123:3051–3060. https://doi.org/10.1029/2018JE005727ExpressMeasurements

Rosenblatt P, Charnoz S, Dunseath KM et al (2016) Accretion of Phobos and Deimos in an extended debris disc stirred by transient moons. Nat Geosci 9:581–583. https://doi.org/10.1038/ngeo2742

Ruhunusiri S et al (2016) MAVEN observations of partially developed Kelvin-Helmholtz vortices at Mars. Geophys Res Lett. https://doi.org/10.1002/2016GL068926

Saito Y et al (2010) In-flight performance and initial results of plasma energy angle and composition experiment (PACE) on SELENE (Kaguya). Space Sci Rev 154(1–4):265–303. https://doi.org/10.1007/s11214-010-9647-x

Saito Y et al (2020) Pre-flight calibration and near-earth commissioning results of the mercury plasma particle experiment (MPPE) onboard MMO (Mio). Space Sci Rev (accepted).

Sakai S, Seki K, Terada N, Shinagawa H, Tanaka T, Ebihara Y (2018) Effects of a weak intrinsic magnetic field on atmospheric escape from Mars. Geophys Res Lett 45:9336–9343. https://doi.org/10.1029/2018GL079972

Sakata R, Seki K, Sakai S, Terada N, Shinagawa H, Tanaka T (2020) Effects of an intrinsic magnetic field on ion loss from ancient Mars based on multispecies MHD simulations. J Geophys Res Space Phys 125:e2019JA026945. https://doi.org/10.1029/2019JA026945

Sánchez-Lavega A, Chen-Chen H, Ordoñez-Etxeberria I et al (2018) Limb clouds and dust on Mars from images obtained by the Visual Monitoring Camera (VMC) onboard Mars Express. Icarus 299:194–205. https://doi.org/10.1016/j.icarus.2017.07.026

Savijärvi H, McConnochie TH, Harri A-M, Paton M (2019) Annual and diurnal water vapor cycles at Curiosity from observations and column modeling. Icarus 319:485–490

Schneider NM, Deighan JI, Jain SK et al (2015) Discovery of diffuse aurora on Mars. Science 350:1–6. https://doi.org/10.1126/science.aad0313

Segura TL, Toon OB, Colaprete A, Zahnle K (2002) Environmental effects of large impacts on Mars. Science 298:1977–1980. https://doi.org/10.1126/science.1073586

Segura TL, Toon OB, Colaprete A (2008) Modeling the environmental effects of moderate-sized impacts on Mars. J Geophys Res Planets. https://doi.org/10.1029/2008JE003147

Sharaf O, Amiri S, AlDhafri S et al (2020) Sending hope to Mars. Nat Astron 4:722. https://doi.org/10.1038/s41550-020-1151-y

Shaposhnikov DS, Medvedev AS, Rodin AV, Hartogh P (2019) Seasonal water "pump" in the atmosphere of Mars: vertical transport to the thermosphere. Geophys Res Lett 46:4161–4169. https://doi.org/10.1029/2019GL082839

Shizgal BD, Arkos GG (1996) Nonthermal escape of the atmospheres of Venus, Earth, and Mars. Rev Geophys 34(4):483–505. https://doi.org/10.1029/96RG02213

Shearer CK, McKay G, Papike JJ, Karner JM (2006) Valence state partitioning of vanadium between olivine-liquid: estimates of the oxygen fugacity of Y980459 and application to other olivine-phyric Martian basalts. Am Miner 91(10):1657–1663

Smith MD (2002) The annual cycle of water vapor on Mars as observed by the Thermal Emission Spectrometer. J Geophys Res 107:1–19. https://doi.org/10.1029/2001JE001522

Smith MD (2004) Interannual variability in TES atmospheric observations of Mars during 1999–2003. Icarus 167:148–165. https://doi.org/10.1016/j.icarus.2003.09.010

Smith DE, Zuber MT, Frey HV, Garvin JB, Head JW, Muhleman DO, Pettengill GH, Phillips RJ, Solomon SC, Jay Zwally H, Bruce Banerdt W, Duxbury TC, Golombek MP, Lemoine FG, Neumann GA, Rowlands DD, Aharonson O, Ford PG, Ivanov AB, Johnson CL, McGovern PJ, Abshire JB, Afzal RS, Sun X (2001) Mars Orbiter Laser Altimeter: experiment summary after the first year of global mapping of Mars. J Geophys Res Planets 106(E10):23689–23722. https://doi.org/10.1029/2000JE001364

Spanovich N, Smith M, Smith P et al (2006) Surface and near-surface atmospheric temperatures for the Mars Exploration Rover landing sites. Icarus 180:314–320. https://doi.org/10.1016/j.icarus.2005.09.014

Spiga A, Forget F (2009) A new model to simulate the Martian mesoscale and microscale atmospheric circulation: validation and first results. J Geophys Res 114:1–26. https://doi.org/10.1029/2008JE003242

Spiga A, Faure J, Madeleine J-B et al (2013) Rocket dust storms and detached dust layers in the Martian atmosphere. J Geophys Res Planets 118:746–767. https://doi.org/10.1002/jgre.20046

Steakley K, Murphy J, Kahre M et al (2019) Testing the impact heating hypothesis for early Mars with a 3-D global climate model. Icarus 330:169–188. https://doi.org/10.1016/j.icarus.2019.04.005

Stenberg G, Nilsson H, Futaana Y, Barabash S, Fedorov A, Brain D (2011) Observational evidence of alpha particle capture at Mars. Geophys Res Lett 38:L09101. https://doi.org/10.1029/2011GL047155

Stephant A, Garvie LAJ, Mane P, Hervig R, Wadhwa M (2018) Terrestrial exposure of a fresh Martian meteorite causes rapid changes in hydrogen isotopes and water concentrations. Sci Rep 8:12385. https://doi.org/10.1038/s41598-018-30807-w

Stern JC, Sutter B, Freissinet C et al (2015) Evidence for indigenous nitrogen in sedimentary and aeolian deposits from the Curiosity rover investigations at Gale crater, Mars. PNAS 112:4245–4250. https://doi.org/10.1073/pnas.1420932112

Stone SW, Yelle RV, Benna M et al (2020) Hydrogen escape from Mars is driven by seasonal and dust storm transport of water. Science 370:824–831. https://doi.org/10.1126/science.aba5229

Sugiura N, Hoshino H (2000) Hydrogen-isotopic compositions in Allan Hills 84001 and the evolution of the Martian atmosphere. Meteorit Planet Sci 35:373–380. https://doi.org/10.1111/j.1945-5100.2000.tb01783.x

Terada N et al (2009) Atmosphere and water loss from early mars under extreme solar wind and extreme ultraviolet conditions. Astrobiology 9:1. https://doi.org/10.1089/ast.2008.0250

Ogohara *et al. Earth, Planets and Space*   (2022) 74:1

Page 31 of 32

Thomas N, Cremonese G, Ziethe R, Gerber M, Brändli M, Bruno G, Erismann M, Gambicorti L, Gerber T, Ghose K, Gruber M, Gubler P, Mischler H, Jost J, Piazza D, Pommerol A, Rieder M, Roloff V, Servonet A, Trottmann W, Uthaicharoenpong T, Zimmermann C, Vernani D, Johnson M, Pelò E, Weigel T, Viertl J, Roux ND, Lochmatter P, Sutter G, Casciello A, Hausner T, Veltroni IF, Deppo VD, Orleanski P, Nowosielski W, Zawistowski T, Szalai S, Sodor B, Tulyakov S, Troznai G, Banaskiewicz M, Bridges JC, Byrne S, Debei S, El-Maarry MR, Hauber E, Hansen CJ, Ivanov A, Keszthelyi L, Kirk R, Kuzmin R, Mangold N, Marinangeli L, Markiewicz WJ, Massironi M, McEwen AS, Okubo C, Tornabene LL, Wajer P, Wray JJ (2017) The colour and stereo surface imaging system (CaSSIS) for the ExoMars trace gas orbiter. Space Sci Rev 212:1897–1944. https://doi.org/10.1007/s11214-017-0421-1

Tian F, Claire MW, Haqq-Misra JD, Smith M, Crisp DC, Catling D, Zahnle K, Kasting JF (2010) Photochemical and climate consequences of sulfur outgassing on early Mars. Earth Planet Sci Lett 295(3–4):412–418

Titov DV (2002) Water vapour in the atmosphere of Mars. Adv Space Res 29:183–191. https://doi.org/10.1016/S0273-1177(01)00568-3

Trokhimovskiy A, Fedorova A, Korablev O et al (2015) Mars' water vapor mapping by the SPICAM IR spectrometer: five martian years of observations. Icarus 251:50–64. https://doi.org/10.1016/j.icarus.2014.10.007

Trotignon JG, Mazelle C, Bertucci C, Acuña MH (2006) Martian shock and magnetic pile-up boundary positions and shapes determined from the Phobos 2 and Mars Global Surveyor data sets. Planet Space Sci 54(4):357–369. https://doi.org/10.1016/j.pss.2006.01.003

Tsunakawa H, Shibuya H, Takahashi F, Shimizu H, Matsushima M, Matsuoka A, Nakazawa S, Otake H, Iijima Y (2010) Lunar magnetic field observation and initial global mapping of lunar magnetic anomalies by MAP-LMAG onboard SELENE (Kaguya). Space Sci Rev 154:219–251. https://doi.org/10.1007/s11214-010-9652-0

Turbet M, Tran H, Pirali O, Forget F, Boulet C, Hartmann JM (2019) Far infrared measurements of absorptions by CH_4+CO_2 and H_2+CO_2 mixtures and implications for greenhouse warming on early Mars. Icarus 321:189–199

Turbet M, Gillmann C, Forget F, Baudin B, Palumbo A, Head J, Karatekin O (2020a) The environmental effects of very large bolide impacts on early Mars explored with a hierarchy of numerical models. Icarus 335:113419

Turbet M, Boulet C, Karman T (2020b) Measurements and semi-empirical calculations of CO_2+CH_4 and CO_2+H_2 collision-induced absorption across a wide range of wavelengths and temperatures. Application for the prediction of early Mars surface temperature. Icarus 346:113762. https://doi.org/10.1016/j.icarus.2020.113762

Urata RA, Toon OB (2013) Simulations of the martian hydrologic cycle with a general circulation model: Implications for the ancient martian climate. Icarus 226:229–250. https://doi.org/10.1016/j.icarus.2013.05.014

Usui T, Alexander CM, Wang J, Simon JI, Jones JH (2012) Origin of water and mantle–crust interactions on Mars inferred from hydrogen isotopes and volatile element abundances of olivine-hosted melt inclusions of primitive shergottites. Earth Planet Sci Lett 357–358:119–129. https://doi.org/10.1016/j.epsl.2012.09.008

Usui T, Alexander CM, Wang J, Simon JI, Jones JH (2015) Meteoritic evidence for a previously unrecognized hydrogen reservoir on Mars. Earth Planet Sci Lett 410:140–151. https://doi.org/10.1016/j.epsl.2014.11.022

Usui T (2019a) What geology and mineralogy tell us about water on Mars. In: Yamagishi A, Kakegawa T, Usui T (eds) Astrobiology. Springer, Heidelberg, p 345

Usui T (2019b) Hydrogen reservoirs in Mars as revealed by Martian meteorites. In: Filiberto J, Schwenzer SP (ed) Volatiles in the Martian crust, Elsevier, pp 71–88. https://doi.org/10.1016/B978-0-12-804191-8.00004-0

Usui T, Bajo K, Fujiya W et al (2020) The importance of phobos sample return for understanding the Mars-Moon System. Space Sci Rev 216:49. https://doi.org/10.1007/s11214-020-00668-9

Vago J, Witasse O, Svedhem H, Baglioni P, Haldemann A, Gianfiglio G, Blancquaert T, McCoy D, de Groot R (2015) ESA ExoMars Program: the next step in exploring Mars. Sol Syst Res 49(7):518–528. https://doi.org/10.1134/S0038094615070199

Vaisberg O, Smirnov V (1986) The Martian magnetotail. Adv Space Res 6:301–304

Vandaele AC, Lopez-Moreno JJ, Patel MR et al (2018) NOMAD, an integrated suite of three spectrometers for the ExoMars trace gas mission: technical description, science objectives and expected performance. Space Sci Rev 214:80. https://doi.org/10.1007/s11214-018-0517-2

Vandaele AC, Korablev O, Daerden F, Aoki S, Thomas IR, Altieri F, Lopez-Valverde M, Villanueva G, Liuzzi G, Smith MD, Erwin J, Trompet L, Fedorova AA, Montmessin F, Trokhimovskiy A, Belyaev D, Ignatiev N, Luginin M, Olsen K, Baggio L, Alday J, Bertaux J-L, Betsis DS, Bolsée D, Clancy R, Cloutis E, Depiesse C, Funke B, Garcia-Comas M, Gérard J-C, Giuranna M, Gonzalez-Galindo G, Grigoriev A, Ivanov Y, Kaminski J, Karatekin O, Lefèvre F, Lewis S, Lopez-Puertas M, Mahieux A, Maslov I, Mason J, Mumma M, Neary L, Neefs E, Patrakeev A, Patsaev D, Ristic B, Robert S, Schmidt F, Shakun A, Teanby N, Viscardy S, Willame Y, Whiteway J, Wilquet V, Wolff M, Bellucci G, Patel M, Lopez-Moreno JJ, Forget F, Wilson C, Svedhem H, Vago J, Rodionov D (2019) Martian dust impact on atmospheric H_2O and D/H observed by ExoMars Trace Gas Orbiter. Nature 568(7753):517–520. https://doi.org/10.1038/s41586-019-1096-4

Vasilyev AV, Mayorov BS, Bibring JP (2009) The retrieval of altitude profiles of the Martian aerosol microphysical characteristics from the limb measurements of the Mars Express OMEGA spectrometer. Sol Syst Res 43:392–404. https://doi.org/10.1134/S0038094609050025

Vincendon M, Pilorget C, Gondet B et al (2011) New near-IR observations of mesospheric CO_2 and H_2O clouds on Mars. J Geophys Res Planets 116:1–18. https://doi.org/10.1029/2011JE003827

Wadhwa M (2001) Redox state of Mars' upper mantle and crust from Eu anomalies in shergottite pyroxenes. Science 291(5508):1527–1530

Wang H, Ingersoll AP (2002) Martian clouds observed by Mars Global Surveyor Mars Orbiter Camera. J Geophys Res 107:1–16. https://doi.org/10.1029/2001JE001815

Webster CR, Mahaffy PR, Flesch GJ et al (2013) Isotope ratios of H, C, and O in CO_2 and H_2O of the Martian atmosphere. Science 341:260–263. https://doi.org/10.1126/science.1237961

Wilson RJ, Neumann GA, Smith MD (2007) Diurnal variation and radiative influence of Martian water ice clouds. Geophys Res Lett 34:1–4. https://doi.org/10.1029/2006GL027976

Witasse O, Duxbury T, Chicarro A, Altobelli N, Andert T, Aronica A, Barabash S, Bertaux JL, Bibring JP, Cardesin-Moinelo A, Cichetti A, Companys V, Dehant V, Denis M, Formisano V, Futaana Y, Giuranna M, Gondet B, Heather D, Hoffmann H, Holmström M, Manaud N, Martin P, Matz KD, Montmessin F, Morley T, Mueller M, Neukum G, Oberst J, Orosei R, Pätzold M, Picardi G, Pischel R, Plaut JJ, Reberac A, Pardo Voss P, Roatsch T, Rosenblatt P, Remus S, Schmedemann N, Willner K, Zegers T (2014) Mars Express investigations of Phobos and Deimos. Planet Space Sci 102:18–34. https://doi.org/10.1016/j.pss.2013.08.002

Wong MH, Atreya SK, Mahaffy PN et al (2013) Isotopes of nitrogen on Mars: atmospheric measurements by Curiosity's mass spectrometer. Geophys Res Lett 40:6033–6037. https://doi.org/10.1002/2013GL057840

Wordsworth R, Forget F, Millour E et al (2013) Global modelling of the early martian climate under a denser CO_2 atmosphere: Water cycle and ice evolution. Icarus 222:1–19. https://doi.org/10.1016/j.icarus.2012.09.036

Wordsworth RD, Kerber L, Pierrehumbert RT et al (2015) Comparison of "warm and wet" and "cold and icy" scenarios for early Mars in a 3-D climate model. J Geophys Res Planets 120:1201–1219. https://doi.org/10.1002/2015JE004787

Wordsworth R, Kalugina Y, Lokshtanov S et al (2017) Transient reducing greenhouse warming on early Mars. Geophys Res Lett 44:665–671. https://doi.org/10.1002/2016GL071766

Xu S, Mitchell D, Luhmann J et al (2017) High-altitude closed magnetic loops at Mars observed by MAVEN. Geophys Res Lett 44:11229–11238. https://doi.org/10.1002/2017GL075831

Yamauchi M et al (2015) Seasonal variation of Martian pick-up ions: evidence of breathing exosphere. Planet Space Sci 119:54–61

Yokota S, Saito Y, Asamura K, Mukai T (2005) Development of an ion energy mass spectrometer for application on board three-axis stabilized spacecraft. Rev Sci Instrum 76:014501. https://doi.org/10.1063/1.1834697

Yokota S, Kasahara S, Mitani T et al (2017) Medium-energy particle experiments–ion mass analyzer (MEP-i) onboard ERG (Arase). Earth Planets Space. https://doi.org/10.1186/s40623-017-0754-8

Yokota S, Terada N, Matsuoka A, Murata N, Saito Y, Delcourt D, Futaana Y, Seki K, Schaible MJ, Asamura K, Kasahara S, Nakagawa H, Nishino MN, Nomura R, Keika K, Harada Y (2021) In situ observations of ions and magnetic field around Phobos: The Mass Spectrum Analyzer (MSA) for the Martian Moons eXploration (MMX) mission. Earth Planets Space. https://doi.org/10.1186/s40623-021-01452-x

Zurek RW, Smrekar SE (2007) An overview of the Mars Reconnaissance Orbiter (MRO) science mission. J Geophys Res 112:1–22. https://doi.org/10.1029/2006JE002701